# Influence of the Wall Temperatures of the Combustion Chamber and Intake Ports on the Charge Temperature and Knock Characteristics in a Spark-Ignited Engine

Seokwon Cho[1], Chiheon Song[1], Namho Kim [1], Sechul Oh[1], Dong Han[2] and Kyoungdoug Min[1*]

## Abstract

Reducing wall temperatures is a promising method to suppress knocking behavior in spark-ignited engine. However, this may increase undesirable heat loss which acts as countereffect, so a strategic cooling approach is required. In this study, a multidisciplinary investigation of the wall temperature effect was demonstrated using experiments and simulations. By experiments under full load and part load conditions, improvements in the indicated thermal efficiency achieved by knock-limited spark advancement were obtained, and detailed analyses were incorporated. Under cooled conditions, it was found that an improved thermal efficiency was achieved by not only the advanced combustion phasing but also the reduced compression work obtained from increased gas density, particularly under part load conditions. By categorizing and evaluating the heat transfer phases using simulations, it was found that the cooled wall temperature did not provide a significant gas temperature drop via compression and combustion processes. Unexpectedly, a notable contribution to gas heat transfer reduction arose during the early gas induction stage because of not only the extended period of heat transfer but also the large surface area and initial

[1]Department of Mechanical and Aerospace Engineering, Seoul National University, Seoul 08826, Korea

[2]Key Laboratory of Power Machinery and Engineering, Shanghai Jiao Tong University, Shanghai 200240, China

*Corresponding Author:
Professor Kyoungdoug Min, Seoul National University, Seoul 08826, Korea
e-mail: kdmin@snu.ac.kr

low temperature before compression. An enhanced cooling on cylinder head resulted in a larger effect on knock mitigation than enhanced liner cooling under normal conditions, attributed to the large heat transfer at the intake port wall. From the assessment, as the liner coolant dominated the piston surface, it was found that the contribution of the liner wall temperature to the gas temperature reduction was significantly influential, even showing a higher knock mitigation effect after intake port insulation was applied. Intensified tumble flow showed a high potential of gas temperature decrease by increasing the heat transfer from gas to wall during the compression stroke, and the effect of the enhanced cooling on the liner was more significant than that of the normal intake port due to the high velocity and turbulence of the air. The simulation results revealed that enhanced liner cooling could decrease the in-cylinder temperature by more than 18 K when insulation and intensification were both applied to the intake port design.

## Keywords (6)

Cooling; Knock; Autoignition; Wall temperature; Heat transfer; Engine

## Acronyms

| | |
|---|---|
| 3D | three-dimensional |
| ASTM | American Society for Testing and Materials |
| aTDC | after top dead center |
| BDC | bottom dead center |
| bTDC | before top dead center |
| CA | crank angle |
| CA10 | crank angle at 10% mass fraction burned |
| CA50 | crank angle at 50% mass fraction burned |
| CA90 | crank angle at 90% mass fraction burned |
| CFD | computational fluid dynamics |

| | |
|---|---|
| $CO_2$ | carbon dioxide |
| CVVT | continuous variable valve timing |
| DISI | direct injection spark ignition |
| DOHC | double overhead cam |
| DPI | dual port injection |
| EGR | exhaust gas recirculation |
| EU | European Union |
| EVC | exhaust valve closing |
| EVO | exhaust valve opening |
| fTDC | firing top dead center |
| GDI | gasoline direct injection |
| gIMEP | gross indicated mean effective pressure |
| IGN | ignition |
| IT | inversion timing |
| IVC | intake valve closing |
| IVO | intake valve opening |
| KLSA | knock-limited spark advancement |
| KO | knock onset |
| LHV | low heating value |
| MAPO | maximum amplitude pressure oscillation |
| MBT | maximum brake torque |
| MFB | mass fractioned burned |
| NEDC | New European Driving Cycle |
| nIMEP | net indicated mean effective pressure |
| PFI | port fuel injection |
| PMEP | pumping mean effective pressure |
| PPS | polyphenylene sulfide |
| RANS | Reynolds-averaged Navier-Stokes |
| rpm | revolution per minute |
| SI | spark ignition |
| TDC | top dead center |
| TVE | threshold value exceeded |
| UHC | unburned hydrocarbon |
| WOT | wide open throttle |

# 1. Introduction

Carbon dioxide ($CO_2$) is well known to be the main contributor to greenhouse effects. The contribution to overall $CO_2$ production from the transportation sector comprises approximately 23% [1]. Therefore, global pressure to reduce $CO_2$ production has forced automakers to invest aggressively in innovative technologies. For the regulation of light-duty vehicle $CO_2$, the European Union (EU) mandated 130 g/km in 2015 and 118 g/km in 2016, to be reinforced to 96 g/km in 2021 [2]. The regulation in the EU will mandate a further reduction in $CO_2$ emissions: 15% less in 2025 and 37.5% less in 2030 compared to 2021. Therefore, the achievement of higher thermal efficiency in internal combustion engines is one of the most urgent tasks.

A spark ignition (SI) engine has advantages over other types of internal combustion engines due to its low production cost and simplicity. To fully exploit the potential of these advantages, it is crucial to implement a higher thermal efficiency. Increasing the compression ratio is one of the most practical and promising methods to achieve this goal, as the compression ratio has a direct relationship with the thermal efficiency in an ideal Otto cycle, as shown in equation 1 [3], where $r_c$ is the compression ratio and $k$ is the specific heat ratio. However, a higher compression ratio promotes a knock-prone in-cylinder condition because of the increased pressure and temperature in the unburned end gas region.

$$\eta = 1 - \frac{1}{{r_c}^{k-1}} \quad (1)$$

Knock is the name given to the noise transmitted through the engine structure when spontaneous autoignition occurs in a significant amount of unburned end gas [3]. In an SI engine, as the in-cylinder pressure increases due to compression and combustion, the temperature of the unburned end gas region increases. Hereafter, hot spots in the end gas, located near the flame front, start to autoignite before the flame arrives and lead to a spontaneous rapid heat release of the rest of the end gas. The pressure wave generated by the spontaneous autoignition hits the wall inside

of the cylinder, which causes a pinging sound. If the amount of heat released from knocking combustion is inordinately large, it can cause erosion and damage to engine components such as piston ringland fracture, head gasket leakage, and bore scuffing [1]. Therefore, knock occurrence in SI engines must be avoided during engine operation, and this is the main hindrance of increasing the compression ratio for developing future high-efficiency engines.

Various methodologies have been proposed to mitigate knock in SI engines. Among the methods, some practical approaches in recent studies are introduced in this section. The first approach is to reduce the combustion duration. By reducing the combustion duration, the air-fuel mixture in the unburned gas region can be consumed by deflagration before the in-cylinder condition reaches to the critical point of autoignition. To shorten the combustion duration, intensified tumble and advanced ignition systems have been principally proposed. Intensified tumble [4-12] promotes a higher flame speed by increasing the turbulent kinetic energy. The intensified tumble is realized by an intake port and piston crown design that helps generate and preserve a coherent flow structure.

Advanced ignition systems such as corona discharge ignition [13, 14], plasma ignition [15] and prechamber ignition [16] have been widely investigated in the field, showing remarkable effects on the initial flame growth speed. These systems have a high compatibility with an extremely diluted condition achieved with an exhaust gas recirculation (EGR) system due to its higher ignitability. EGR is now also being actively adopted in mass-produced SI engines alongside the technological development in the advanced ignition system as well as an intensified port design that enables highly diluted combustion to be stable.

Introducing cooled EGR into the cylinder [4, 12] is another effective method for knock suppression, and various fundamental studies have been performed to investigate the corresponding results [17]. Three main impacts of EGR addition on the combustion process are the dilution effect, thermal-diffusion effect and chemical effect [18]. In addition to the largest contribution from dilution, a lower specific heat ratio (thermal-diffusion effect) [19] helps

reduce the end gas temperature during combustion, which decreases the gas reactivity (chemical effect) and heat transfer loss as well.

Introducing gasoline direct injection (GDI) has been proved to be remarkably effective for knock suppression. It increases the charge cooling effect by delivering the fuel in the liquid phase directly into the cylinder; this extends the knock limit [20]. In addition, it can provide a better scavenging process, which was avoided with PFI [21]. Additionally, the GDI engine has more flexibility in its injection splitting and timing, which enables fuel stratification [22] with retarded injection timing [23] to prolong the mixture ignition delay.

Another favorable option that has been proposed for knock mitigation is engine cooling [24]. With a modest change in the engine design, an increase in thermal efficiency can be achieved by the knock suppression effect. There have been practical approaches to enhance the cooling of the end gas, such as engine wall thickness reduction and coolant flow increase. Table 1 is a brief categorization of previous studies that mainly focused on cooling strategy and knock mitigation in the internal combustion engine field. Previous research could not be thoroughly introduced due to the space limitations in this paper. Additionally, the references have intersections to each other and broader coverage but the key features and findings were categorized. Detailed descriptions for important references are followed from the next paragraph.

**Table 1.** Categories and main content of papers regarding engine cooling and knock

| Strategy | Impact, finding and features | Reference |
|---|---|---|
| Dual circuit cooling | Importance of head coolant temperature | Kobayashi et al., 1984 [25] |
| | Knock limit improvement | Fukuda et al., 2004 [26] |
| | Efficiency increase, knock limit extension | Rehman and Sarviya, 2010 [27] |
| | Knock suppression, heat loss decrease, production engine | Hwang et al., 2016 [4] |
| | Efficiency increase, knock suppression, production engine | Matsuo et al., 2016 [28] |
| | Knock suppression | Cho et al., 2018 [29] |
| Evaporative cooling | Increased heat transfer, knock suppression | Kubozuka et al., 1987 [30] |
| | Warm-up time reduction, efficiency increase | Clough, 1993 [31] |

| | | |
|---|---|---|
| Precision cooling | Flow rate reduction of coolant | Finlay et al., 1988 [32] |
| | Knock suppression | Iwashita et al., 1989 [33] |
| | Effective knock suppression, KLSA advancement | Nishino et al., 2004 [34] |
| | Production engine, efficiency increase, knock suppression | Shibata et al., 2017 [35] |
| Regular cooling | Knock suppression | Sanders and Peters, 1945 [36] |
| | Knock suppression | Shiga et al., 1990 [37] |
| | Quantification of knock mitigation effect | Russ, 1996 [38] |
| | KLSA advancement (no effect) | Asif et al., 2017 [39] |
| | Knock suppression, knock location | Cho et al., 2017 [40] |
| | Knock suppression | Perrone et al., 2019 [41] |
| Heat transfer analysis | Impact of liner wall temperature and exhaust side | Takahashi et al., 2012 [42] |
| | Impact of intake port insulation, knock suppression | Imaoka et al., 2016 [43] |
| Review | A review for cooling technologies as of June 17, 2004 | Pang et al., 2004 [24] |

Kobayashi et al. [25] integrated a dual circuit cooling system with a 1.3 L four-cylinder engine with a compression ratio of 9.0. The result showed that the degree of knock reduction was affected more by the temperature of cylinder head coolant than that of the liner coolant. It was observed that reducing the head coolant temperature was twice as effective in knock mitigation relative to cooling the coolant temperature flowing across the liner. The authors explained that the greatest impact from a reduced head coolant temperature is due to the enhanced cooling of the unburned gas temperature during the combustion process.

Finlay et al. [32] investigated the effect of a precision cooling system with small automotive engines and observed that an increased coolant flow can decrease surface temperatures effectively. Kubozuka et al. [30] introduced an evaporative cooling system. More sophisticated wall temperature control was enabled, and the effect was shown as a 1 CA (crank angle) advance of knock-limited spark advancement (KLSA) achieved per 10 K decrease in the coolant temperature. The developed cooling system showed a larger effect than liquid cooling; a 90-100°C condition showed a similar effect to an 85°C liquid cooling condition. Iwashita et al. [33] also demonstrated that the increased coolant flow in a precision cooling system allows an additional 2-4 CA of ignition timing advance by reducing the wall temperatures.

Russ [38] observed borderline knock characteristics under various engine operating conditions. The author quantified the knock suppression effect of individual operating conditions as a function of octane number. The effect of the coolant temperature was also investigated, and it was quantified that a 10 K drop in the coolant temperature corresponded to an increase in one octane number. Independent cooling of the cylinder head and block was also examined and showed that the corresponding knock mitigation effects were similar in practice. The author indicated that even though the engine head temperature predominantly affected the heat transfer during the intake stroke, the results could be attributed to the large heat addition from the block temperature during the compression stroke. In addition, the cooling strategy showed a more substantial effect under lower engine speed conditions due to the expanded time for heat transfer.

Fukuda et al. [26] employed a dual cooled system with individual thermostats in their 2.4 L double overhead cam (DOHC) research engine. With the dual control system, a 6.3 CA advancement in ignition timing was achieved in addition to a 1.6 CA advancement by reducing wall temperatures by 10 K. As a result, the output torque was improved by 2.5%.

Takahashi et al. [42] conducted three-dimensional (3D) simulation to establish a cooling strategy. The authors explained that heat transfer from the in-cylinder wall to the mixture gas took place mainly at the exhaust side of the liner rather than the intake side due to gas motion at the beginning of the intake process. Imaoka et al. [43] also conducted an investigation related to the heat added from the various parts of the walls, including the intake port wall during the intake process. Both 3D simulation and an experimental approach, by using a few segregated cooling passages, were utilized. The outcome of the study revealed that the heat transfer between the intake port wall and air was a dominant cause for an increasing gas temperature.

Asif et al. [39] investigated the effect of the coolant temperature on KLSA using a multicylinder direct injection spark ignition (DISI) engine with a dual continuous variable valve timing (CVVT) system. The study showed that

a reduction in coolant flow by 20% led to the temperature within the exhaust valve bridge decreasing by only 1 K. The KLSA was retarded from approximately 0.5 to 1 CA when the coolant temperature increased from 90°C to 100°C. The authors explained that this variation cannot be considered a significant change.

Inoue et al. [44] and Morioka et al. [45] conducted extensive experimental studies on the heat transfer effect in the intake port. A resin-coated intake port wall was used to decrease the charge temperature in the combustion chamber by 6-10 K compared to that of a conventional aluminum surface. Based on the test results with a 1.2 L 3-cylinder engine, heat insulation in the intake port resulted in 3.5 kW higher power at higher engine speed and approximately 1% fuel efficiency improvement in the new European driving cycle (NEDC) and Japanese JC08 driving cycle. However, the effect was not significant when cooled-EGR was utilized.

Uozumi et al. [46] studied the effect of the surface roughness of the combustion chamber walls on the knock phenomenon. They investigated the correlation between the parameters of the surface roughness and heat transfer coefficient. The results indicated that a higher surface roughness angle and height could lead to increased heat transfer, mainly due to a higher possibility of air molecule collision on surfaces with increased roughness. They concluded that the reduced heat transfer achieved by the improved unevenness of the surface could result in a reduction in the unburned gas temperature, which facilitated the ignition timing advance. In addition, the surface roughness of the piston had the largest effect on knock mitigation compared to that of other components such as the head, exhaust and intake valves.

Although it is well known that engine cooling can lead to knock suppression, the detailed physical phenomena during the engine cycle have not yet been revealed. In addition, the effect of changing the individual wall temperature on the knock phenomenon and the unburned gas temperature still remains to be demonstrated. Because the thermodynamic condition of the trapped air-fuel mixture is controlled mainly by convective heat transfer, the impact of wall temperature variations on the end gas condition is substantial. A lower wall temperature reduces the

heat transferred to the gas mixture from the engine component walls during the intake stroke. A less heated charge can allow the advancement of ignition timing, leading to efficiency improvement. However, decreasing the wall temperatures can also increase the heat transfer loss to the combustion chamber wall during the combustion and expansion stroke, which counteracts the efficiency improvement achieved from the ignition timing advancement.

Therefore, in this study, a detailed investigation on the impact of the wall temperatures is demonstrated by means of experiments and simulations. A novel approach is made to understand the flow and its heat transfer interaction with walls by splitting the phases. Thus, the effect of the individual engine components is analyzed, enabling a strategic cooling method to be proposed. Furthermore, because intensified tumble flow is now actively adopted for higher thermal efficiency, the wall interaction under this high tumble flow is also investigated.

# 2. Methodology

## 2.1 Experimental setup

A 0.5 L single-cylinder engine based on a 2.0 L production engine was used for the experiment in this study. The bore and stroke were 81 mm and 97 mm, respectively. The target geometric compression ratio was 12; the value measured by the swept volume measurement device was 11.89. The engine was equipped with dual CVVT. The injection system was retrofitted for dual port injection (DPI) for research purposes instead of a single port fuel injection (PFI) injector [47-49]. This system was used to achieve better fuel vaporization, and the injectors actuated synchronously. Except for the dual port fueling, other components and designs, including the valve profiles, were unchanged from the production engine design. The base production engine had 10.4 mm of crankshaft offset primarily for reducing the friction loss, and the offset direction was inclined to the intake side enabling less friction loss to maximize the brake thermal efficiency. The intake setup was fully symmetrical, with no additional swirl. Detailed engine specifications are listed in Table. 2.

**Table 2.** Salient features of the single-cylinder test engine

| | | |
|---|---|---|
| Displacement volume [cc] | | 499.8 |
| Bore [mm] | | 81 |
| Stroke [mm] | | 97 |
| Connecting rod [mm] | | 150.9 |
| Geometric compression ratio | | 11.89[1]:1 |
| Crankshaft offset [mm] | | 10.4 |
| Injection system | | Dual PFI (3.5 bar) |
| Number of valves | | 4 |
| Maximum valve lift [mm] | | 10 |
| Valve Timing (@ 0.1 mm) | EVO/EVC | 68 CA bBDC/1 CA aTDC |
| | IVO/IVC | 10 CA aTDC/67 CA aBDC |

[1] Value measured by a swept volume measurement device [50]

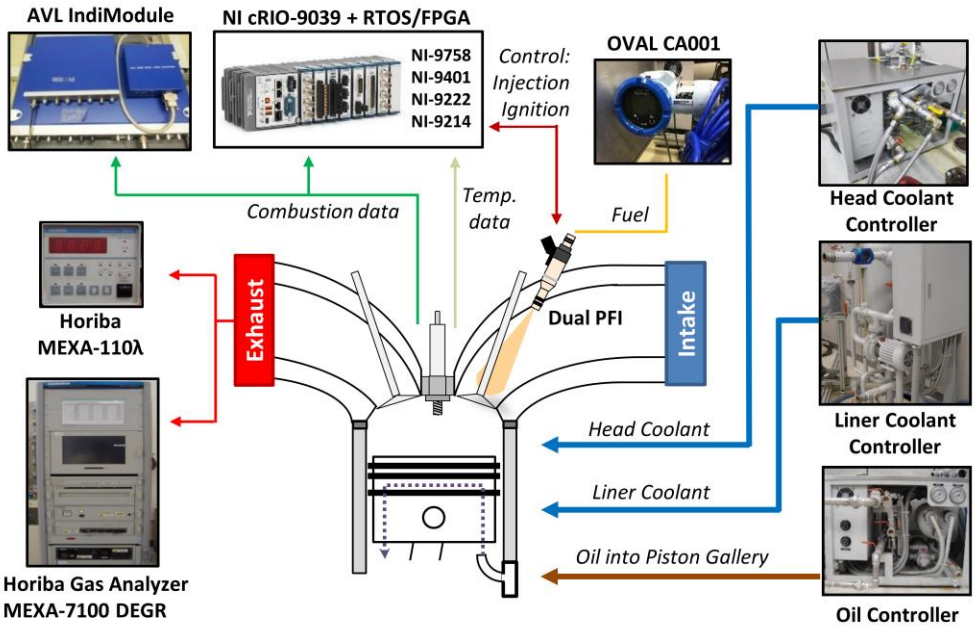


**Fig. 1.** Schematic diagram of the engine experimental facility.

A schematic diagram of the engine experiment is depicted in Fig. 1. A Kistler 6056A piezoelectric in-cylinder pressure sensor was mounted flush into the cylinder with a slightly biased position to capture the in-cylinder pressure oscillation with high sensitivity. The data resolution for pressure data was 0.1 CA, and it was facilitated by using a physical 3600-teeth encoder. The signal from this sensor was amplified using an AVL Micro IFEM. A Kistler 4045A2 piezoresistive pressure sensor was installed in the intake manifold, approximately 100 mm from the intake port surface or the cylinder head, for manifold pressure measurement. A Kistler 4603 piezoresistive amplifier was coupled with the Kistler 4045A2 sensor. The in-cylinder pressure was offset by pegging it into the intake manifold pressure near the intake bottom dead center (BDC). An OVAL CA001 Coriolis fuel flow meter was used, and the three-minute ensemble-averaged value was used for high fidelity and repeatability. The exhaust emission was monitored by a HORIBA MEXA-7100 DEGR gas analyzer, and MEXA-110λ was used for measurement and monitoring of the air-fuel ratio during the experiment. A National Instruments cRIO-9039 chassis and several slot modules utilizing RTOS/FPGA were employed to control the engine by employing in-house code.

To obtain a high-fidelity data, many of attempts were made in this study. Only one pair of in-cylinder pressure sensor and intake pressure sensor were used throughout the whole experimental cases with proper maintenance. A proper pegging process was performed during the experiment, avoiding conducting an experiment in a day with very different atmospheric pressure and temperature. TDC calibration was done under the same wall temperature every time, and the peak motoring pressure was validated within 0.2 bar difference before starting the exploration. In addition, usually the valvetrain is driven by timing belt system in a single-cylinder engine, therefore the cam timing has a slight time-to-time deviation. Therefore, CVVT modules for both intake and exhaust camshafts were introduced in this engine and the actual valve timing was monitored and controlled.

During the engine operation, three thousand consecutive cycles were logged for each case after a fully developed steady-state condition was achieved. Thus, the knock propensity must be kept below 10% to prevent the engine

failure by the long-duration operation. For the calculation of efficiency, not only in-cylinder pressure value accounts for valuable portion, but also the impact of the fuel flow rate is not negligible. Once the system reached a fully developed steady-state condition, 10-minutes (1 Hz, 600 data) ensemble-averaged fuel flow value was logged; this allowed the 95% confidence interval size of $7x10^{-4}$ mg/cycle. Furthermore, back-to-back experiments were implemented during this study. As a result, repeatability error within 0.5% in indicated specific fuel consumption (ISFC) was achieved.

The coolant passages for the cylinder head and the liner were segregated to control the surface temperatures independently [29]. Moreover, both coolants were controlled by high-heat-capacity controllers, as shown in Fig. 1. Both coolant flows were maximized (over 10 L/min) to achieve uniform thermal boundary conditions as much as possible. Consequently, the difference in the coolant temperatures between the inlet and outlet was less than 2 K for both the head and coolant for all operating conditions.

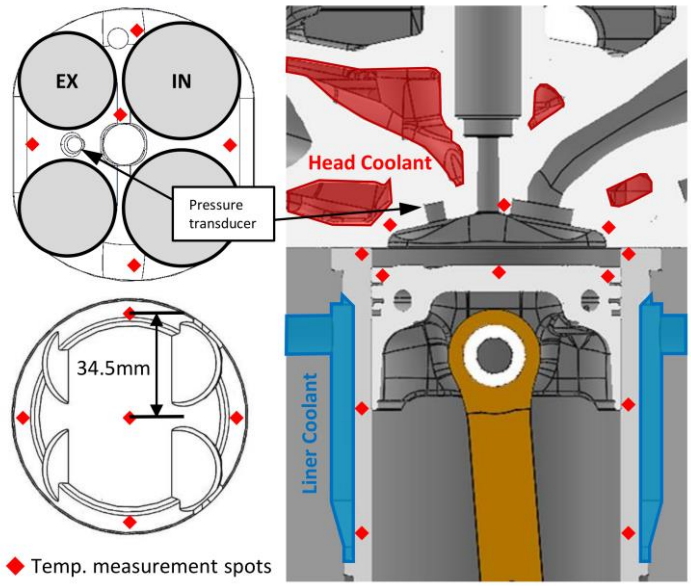


**Fig. 2.** Segregated cooling passage and positions for temperature measurement [29]

Fig. 2 shows a brief design of the engine structure including the segregated cooling passage and temperature measurement points (redrawn from authors' previous study [29]). Twenty-two thermocouples were inserted into various parts of the engine: five points beneath the piston surface, five points in head inner wall and twelve points round in cylinder liner inner wall and on outer wall. The thermocouples were installed 1 mm from the combustion chamber walls to measure the actual surface temperatures as close as possible. The piston temperature measurement was enabled by an optimized linkage system introduced in the authors' previous study [40, 51]. The linkage system design was optimized using an improved downhill simplex optimization (Nelder-Mead method) and 3D stress analysis. The engine was retrofitted with the linkage system after confirming the safety factor of two was achieved at 6000 rpm condition. Special-purpose flexible K-type thermocouple wires (Chromel and Alumel) were used to prevent the fracture during the engine operation.

### 2.2 Engine operating conditions

The experimental conditions are shown in Table. 3. The test was performed at two different engine speeds: 1500 and 2000 rpm. The engine was operated stoichiometrically ($\lambda$=1) under all conditions. Conventional market gasoline fuel with research octane number (RON) 91.5 was used during the experiment. Knock-prone conditions were selected as the operating conditions. To investigate the effect of independent cooling, the coolant temperature of each segregated cooling passage was varied from 60°C to 85°C independently. Decreasing the coolant temperature to 60°C did not show a substantial increase in unburned hydrocarbon (UHC) emission and smoke level, but substantial increases were detected below 60°C even in when the only head coolant was cooled. Particularly, the impact of head coolant decrement was critical due to a poor fuel vaporization process above the intake valves. Therefore, the low limit for coolant temperature in enhanced cooling cases was restricted to 60°C in this study. While the coolant temperatures were varied, the inlet air and oil temperature were unchanged. Fuel was injected well before the intake stroke to provide sufficient time for the liquid fuel to vaporize and promote more homogenous

mixture formation. The injection timing was determined by conducting a brief sweep experiment in 1500 rpm, full load condition. Injecting fuel before 540 CA bTDC led to a decrease in volumetric efficiency. On the other hand, late injection, such as open valve injection, was beneficial for additional knock mitigation. However, it was avoided due to an increase in HC emission in this study. Table 4 shows the properties of the test fuel with the proper testing methods. A conventional gasoline fuel with research octane number (RON) 91.5 was used in this study.

**Table 3.** Experimental conditions

| | |
|---|---|
| Engine speed [rpm] | 1500, 2000 |
| Air-fuel ratio | Stoichiometric ($\lambda = 1$) |
| Load | Part, full (WOT) |
| Ignition timing | KLSA |
| Injection timing | 540 CA bTDC[1] |
| Head coolant temp. [°C] | 60 – 85 |
| Liner coolant temp. [°C] | 60 – 85 |
| Oil temp. [°C] | 75 ± 1 |
| Ambient air temp. [°C] | 30 ± 0.5 |
| Fuel inlet temp. [°C] | 35 ± 2 |
| Knock incidence at KLSA [%] | 10 |

[1] 540 CA before firing TDC

**Table 4.** Test fuel properties

| Property | | Value | Test method |
|---|---|---|---|
| H/C ratio | | 2.064 | ASTM D 5291 |
| Density [kg/m$^3$] at 15°C | | 724.5 | ASTM D 1298 |
| RON | | 91.5 | ASTM D 2699 |
| LHV [MJ/kg] | | 42.825 | ASTM D 240-14 |
| Oxygenate [mass %] | | 1.53 | ASTM D 4815 |
| Distillation Temperature [°C] | Initial boiling point | 38 | ASTM D 86-12 |
| | 10% | 55 | |
| | 50% | 83 | |

| | | | |
|---|---|---|---|
| | 90% | 142 | |
| | End point | 197.6 | |

For knock detection during the experiment, the maximum amplitude of pressure oscillation (MAPO) [52] incidence method (shown in equation 2) was used [29]. Because this study focuses on the relationship between thermal boundary conditions and combustion behavior, a relatively weak knock threshold was chosen not only to prevent engine failure by knocking combustion but also to acquire a sufficient amount of data in such harsh conditions. By using a high-pass filter with nine-point median filtering in equations 3 and 4, a 0.5 bar threshold value exceeded (TVE) method as expressed in equation 5 was adopted for knocking cycle detection [53]. The KLSA in this study was defined as the ignition timing at which the MAPO knock incidence reached 10%. Data from a minimum of one thousand consecutive cycles were monitored to characterize the knock propensity.

$$MAPO\ Incidence\ = \frac{N_{knock}}{N_{total}} \times 100\ [\%] \tag{2}$$

$$P_{med,n} = (P_{n-4} + P_{n-3} + \cdots + P_{n+3} + P_{n+4})/9 \tag{3}$$

$$P_{filt} = P - P_{med} \tag{4}$$

$$\left|P_{filt}\right| > 0.5\ bar \tag{5}$$

### 2.3 Simulation configuration

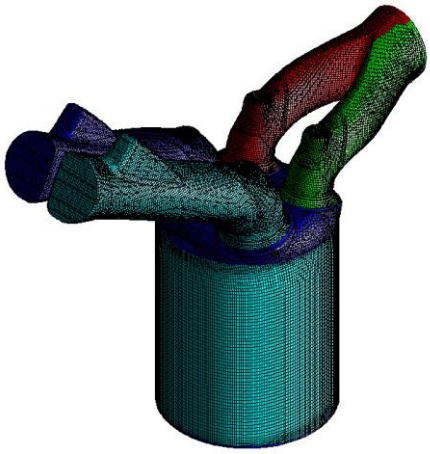

**Fig. 3**. Engine mesh generated at BDC.

To further investigate the heat transfer between the walls and the in-cylinder gas mixture, commercial software, STAR-CD V4.24, was used to conduct 3D computational fluid dynamics (CFD) Reynolds-averaged Navier-Stokes equations (RANS) simulation. The engine mesh used for the simulations is shown in Fig. 3. The grid size of the intake and exhaust region near the boundaries was refined to 1.5 mm, and the discretization near spark plug and valves was 0.5 mm. The number of mesh cells was approximately 1.12 million at BDC. The RNG-k-ε model and Angelberger model [54] were used to simulate the turbulence and wall heat transfer, respectively. Extended coherent flame model for three zones (ECFM-3Z) model was used for the combustion model. As the scope of this study is to analyze heat transfer between the walls and the charge, reasonable y+ values were required. As a result, y+ predictions are similar in each wall part, and the values were in 20 to 100 range. The numerical quantities of convergence criteria were: pressure $10^{-4}$, velocity $10^{-3}$, temperature $10^{-3}$, TKE/EPS $10^{-3}$.

Table 5 lists the surface temperatures used for the simulations. In this study, simulations were performed under both motored and fired conditions; the firing condition was introduced to check the impact of change in heat transfer during the combustion period. This will be explained more in detail later in this study. For the thermal boundary

setup, the experimental result from 1500 rpm, wide-open throttle (WOT) was used as the baseline. From the baseline condition, each case in the table shows a 20 K decrease in the surface temperature of each component. The intake valve stem temperature was set as 15 K above the intake port wall temperature, and the intake valve face was set at the same temperature as the head surface in this study. The surface temperatures of the exhaust valves and spark plugs remained unchanged, as reported by French et al. [3, 55]. The temperature of the exhaust valve surfaces was fixed at 580 K, and that of the spark plug was held at 600 K. The case with enhanced liner cooling also shows a lower temperature of the piston surface despite the piston not being actively cooled. This is because the piston surface temperature was correlated with the liner wall temperature. This topic is discussed later in the paper. The validation was done using the data from case 1 matching the in-cylinder pressure. The intake pressure trace obtained from the experiment was used for the boundary condition.

**Table 5**. Case description and corresponding wall temperatures used for simulations

| Case # | Name | Head [°C] | Liner [°C] | Piston [°C] | Intake Port [°C] |
|---|---|---|---|---|---|
| 1 | Baseline | 115 | 110 | 165 | 85 |
| 2 | Liner ↓ | 115 | 90 | 154 | 85 |
| 3 | Head ↓ | 95 | 110 | 165 | 60 |
| 4 | All ↓ | 95 | 90 | 154 | 60 |

## 3. Results and discussion

In this study, the directions of the experimental investigation are twofold. First, experimental results under full load and part load conditions accompanied by detailed analyses are shown. Second, the effects of coolant passage segregation and observation are presented. Knock testing results of coolant temperatures of 60°C and 85°C and the related parameter values in this study are summarized in Table A1. As previously mentioned, 3D simulation was also used to further understand the heat transfer interaction.

### 3.1 Knock mitigation and its effect on the energy balance

In this experiment, the coolant temperatures applied to both the cylinder head and the block were varied simultaneously while fixing the rate of coolant flow.

#### 3.1.1 Full load conditions

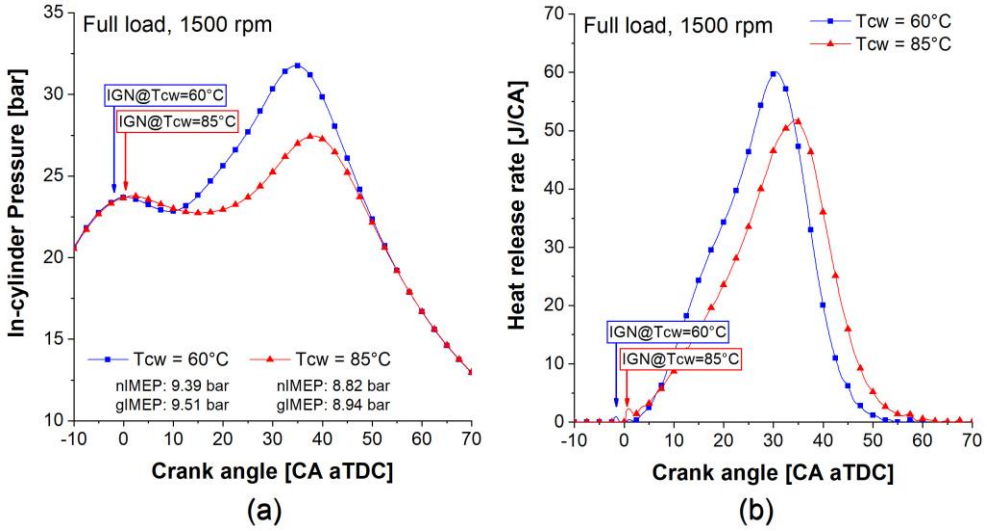


**Fig. 4**. Variation in the in-cylinder pressure curves and heat release rates at 1500 rpm, full load; (a) in-cylinder pressure; (b) heat release rate.

Figures 4(a) and 4(b) show the in-cylinder pressure traces and heat release rates at 1500 rpm under full load conditions. Numeric values from experimental results are summarized in Table A1 in the Appendix section. As the coolant temperature was decreased, the KLSA could be advanced from 2 CA aTDC to 0.4 CA bTDC. To maintain stoichiometric conditions, the amount of fuel input was increased from 31.8 to 32.7 mg/cycle for the lower coolant temperature case. This is a result of the increased trapped air mass as the charge density increases with decreasing coolant temperature.

When the coolant temperature decreases, the heat transfer from the solid walls of the engine components to the inducted air decreases during the intake stroke. This results in prolonged ignition delay of the air-fuel mixture during the compression and combustion processes which enabled the knock suppression. When the coolant temperature was decreased, the expansion work (TDC-EVO) was significantly increased (616.0 to 644.6 J) due to advanced spark timing and corresponding advancement of combustion phasing (CA50) from 32.1 to 28.7 CA aTDC, whereas the compression work (IVC-TDC) was maintained at the same level. Although the charge mass was increased under cooler conditions, the compression work (i.e., negative work) did not change significantly. Additionally, because the intake pressure was unchanged, only a minor difference in the pumping loss was observed. The combustion duration (CA10-90) was shortened from 27.6 to 24.2 CA with the advancement of KLSA and showed a remarkable increase in the expansion work. Subsequently, the net indicated mean effective pressure (nIMEP) was increased from 8.82 to 9.39 bar, and the ISFC was decreased by 3.4% from 259.5 to 250.6 g/kWh.

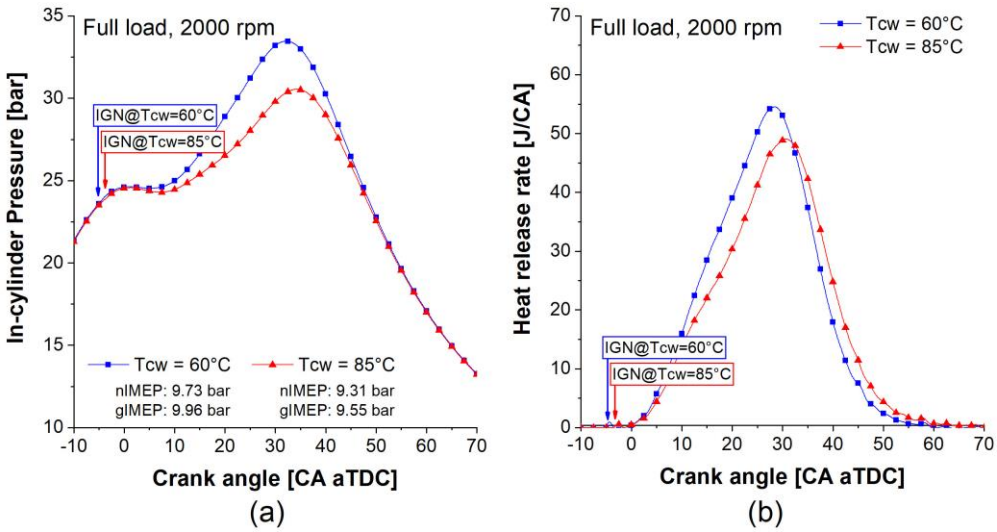


**Fig. 5.** Variation in the in-cylinder pressure curves and heat release rates at 2000 rpm, full load; (a) in-cylinder pressure; (b) heat release rate.

283 Figures 5(a) to 5(b) illustrate the results under the 2000 rpm full load conditions. A similar trend in the
284 experimental results was observed at this engine speed. The maximum load was increased from 9.33 to 9.73 bar of
285 nIMEP by changing the KLSA from 3.3 to 3.9 CA bTDC. Corresponding advance of CA 50 was also observed.
286 Such results can be attributed to a decreased in-cylinder gas temperature by enhanced cooling. No significant change
287 in the pumping loss was observed, and the combustion duration was shortened by 1.4 CA from its original 19.8 CA;
288 thus, the ISFC decreased by 2.18%, from 252.3 to 246.8 g/kWh.

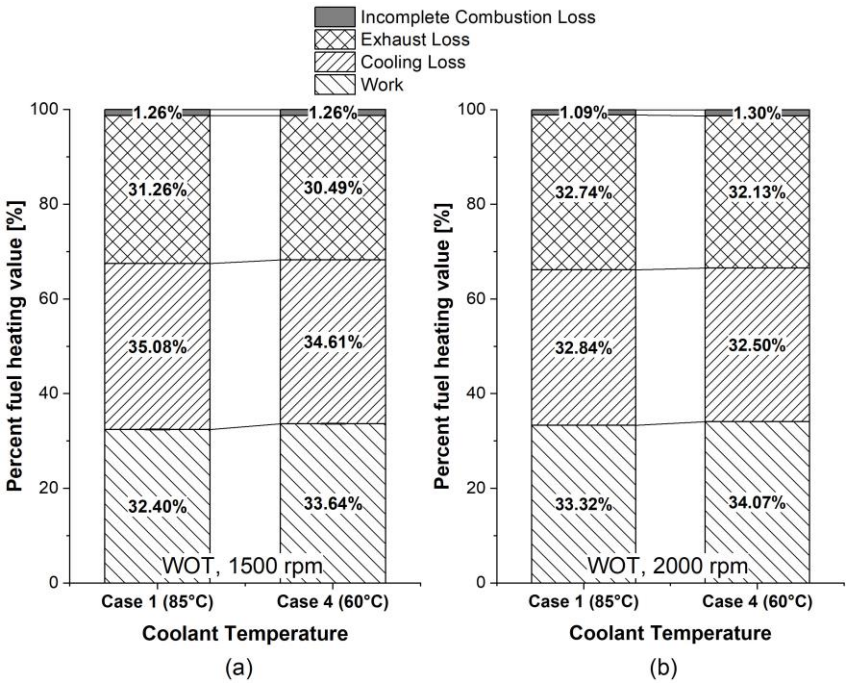

289

290 **Fig. 6**. Low heating value (LHV) breakdown under coolant temperatures of 60 and 85°C; (a) 1500 rpm, full load
291 and (b) 2000 rpm, full load conditions.

292 Fig. 6 displays the fuel energy breakdown (percent fuel heating value) in both the 1500 and 2000 rpm cases. The
293 cooling loss was calculated based on the first law of thermodynamics and knowledge of the work and enthalpy
294 flows [56-58]. That being said, the heat rejection was calculated by subtracting the followings from the total input

fuel energy (LHV): incomplete combustion loss, exhaust enthalpy loss and mechanical (PdV) work. The incomplete combustion loss and the exhaust enthalpy loss were calculated with Matlab/Cantera 2.3.0 toolbox using the exhaust gas composition and the temperature. Due to the advancement of KLSA achieved by lowering the coolant temperature, the exhaust loss was converted to useful work. The percentage of cooling loss was decreased under enhanced cooling conditions of 1.6% to 34.52% at 1500 rpm and 1% to 32.5% at 2000 rpm. However, the total amount of cooling loss was slightly increased with lower coolant temperatures. In enhanced cooling cases, the decreased heat transfer amount to charge from the walls allowed the advancement in KLSA and a significant increase in expansion work. The increased temperature during combustion led to higher heat transfer loss and increased cooling loss.

### 3.1.2 Part load conditions

Under full load operation of modern gasoline SI engines, the ignition timing is generally retarded far from the maximum brake torque (MBT) to avoid knocking combustion. Therefore, the exhaust loss is substantial, so recuperation of the exhaust loss into useful work is crucial for efficiency improvement. In other words, KLSA timing is the most significant factor in determining thermal efficiency. However, under part load conditions, the ignition timings are maintained close to the MBT timings. Thus, further advancement in the ignition timings is very unlikely to contribute to improvement in thermal efficiency. To investigate the role of coolant temperature under part load conditions, additional experiments were conducted. The same engine speeds, 1500 and 2000 rpm, were used as in the full load conditions.

Under both 1500 and 2000 rpm conditions, the operating parameters such as the ignition timing and fuel mass were specified when the KLSA reached MBT timing at the 60°C coolant temperature condition. Subsequently, the KLSA was retarded at 85°C coolant temperature. For all the part load experiments, the mass of fuel was held constant regardless of the coolant temperature. To maintain the same intake air mass for all conditions, the intake

pressure had to be increased as the coolant temperature was increased from 60 to 85°C. This is attributable to the increased charge temperature at the coolant temperature condition that reduces the intake air density.

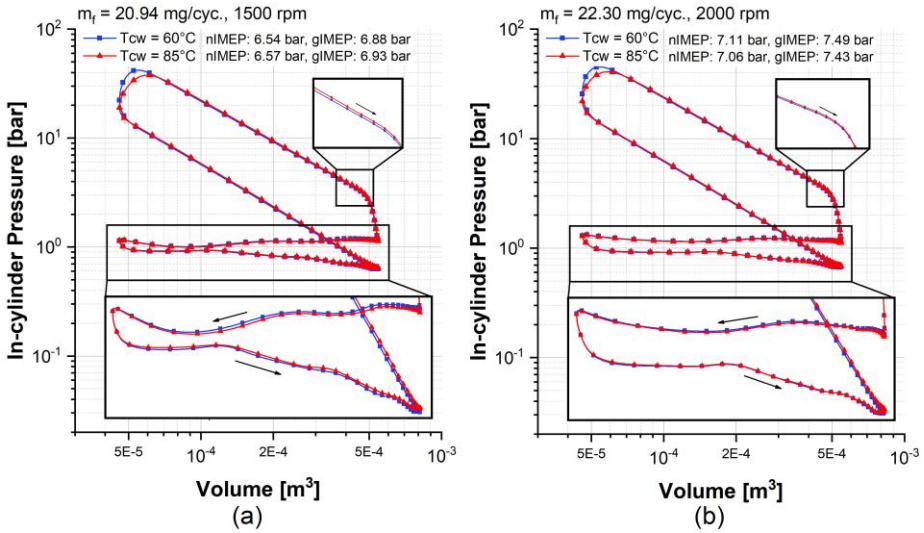


**Fig. 7**. P-V diagram (logarithmic) of part load conditions at (a) 1500 rpm and (b) 2000 rpm.

Figures 7(a) and 7(b) depict the logarithmic-scaled diagrams of pressures as a function of volume (P-V diagram) of the constant fuel input cases at 1500 and 2000 rpm. Necessary values for understanding can also be found in Table A1. As described previously, the KLSA of the 60°C case (blue in the figures) was the MBT timing at the given condition. As expected, the KLSA became more retarded (shown in Table A1) at higher coolant temperature conditions: 19.8 to 15.9 CA bTDC at 1500 rpm and 23.5 to 19.8 CA bTDC at 2000 rpm. Despite the advancement of KLSA, the expansion work did not substantially change: 0.04% and 0.2% at 1500 and 2000 rpm, respectively. This is because the ignition timing was already close to the MBT timing at the given conditions. Thus, such further advancement of ignition timing did not substantially recuperate exhaust loss into useful work. This is also attributable to the work decrease in the expansion stroke; the enhanced cooling cases show less pressure (upper magnified boxes) due to the advanced ignition timing. Increased pumping losses in the enhanced cooling cases are

found in the results; the enhanced cooling cases have a higher pressure during the exhaust process and a lower pressure during the intake process, as shown in the lower magnified boxes.

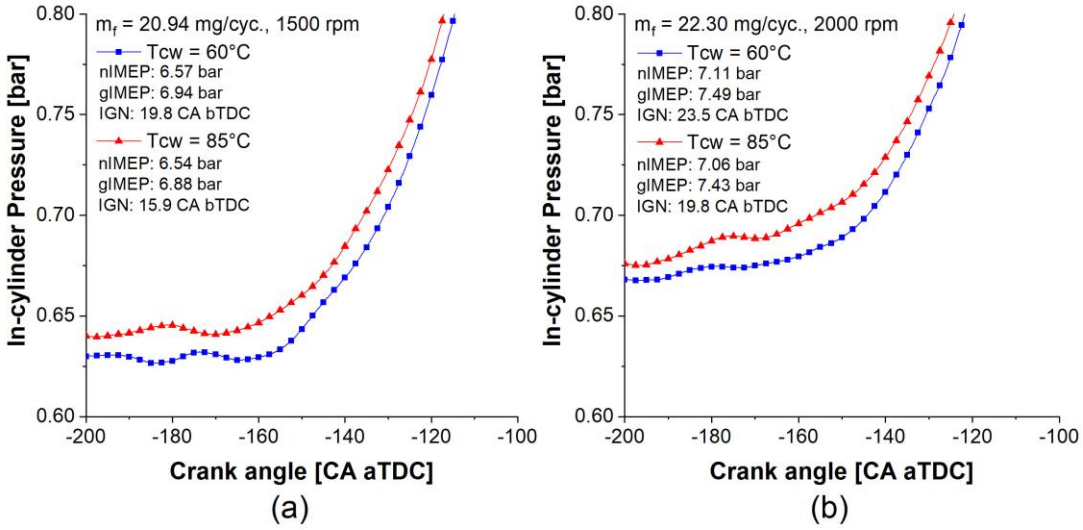


**Fig. 8.** Variation of the in-cylinder pressure curves near intake valve closing (IVC) timing under part load conditions at (a) 1500 rpm and (b) 2000 rpm.

Figures 8(a) and 8(b) show the pressure traces near IVC timing (144 CA bTDC). The pressure during the intake stroke was slightly lower at the 60°C coolant temperature at both engine speeds. This is attributed to the differences in the intake air density, as mentioned earlier. This considerable reduction in intake pressure decreased the compression work (126.0 to 123.4 at 1500 rpm and 135.7 to 133.9 at 2000 rpm); thus, the gross indicated mean effective pressure (gIMEP) increased despite an insignificant increase in the expansion work. This increase arose primarily from the reduced compression work, and this effect was larger than the negative effect of the pumping mean effective pressure (PMEP) increase.

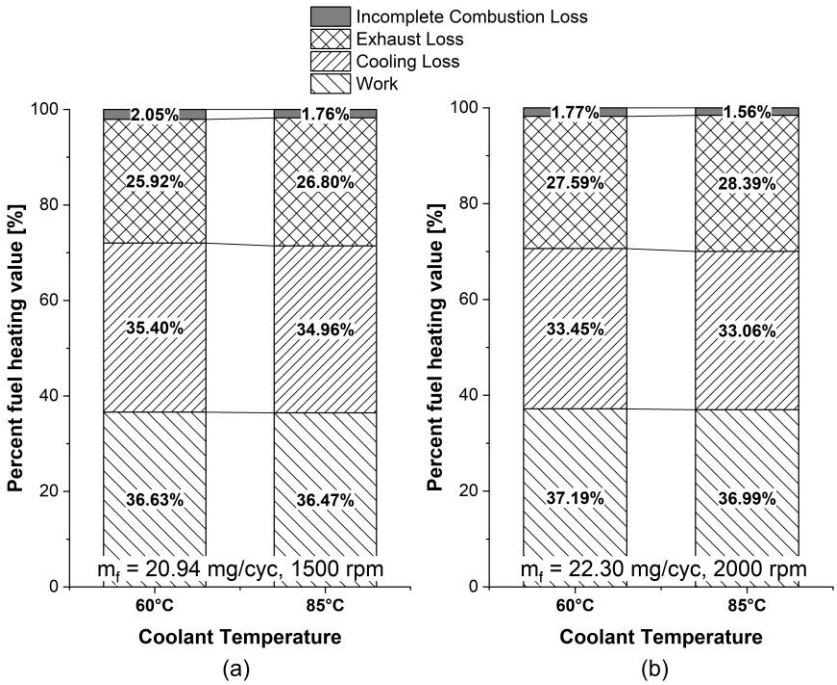


**Fig. 9**. LHV breakdown under coolant temperatures of 60 and 85°C; (a) 1500 rpm, part load and (b) 2000 rpm, part load conditions.

Figures 9(a) and 9(b) illustrate the LHV breakdown from the part load cases. Because the average fuel mass was held constant during the experiments, a side-to-side comparison of the values is feasible. At both engine speeds, the indicated thermal efficiency (ITE) was enhanced when the lower coolant temperature was used: a 0.4% increase to 36.63% at 1500 rpm and a 0.5% increase to 37.19% at 2000 rpm. However, these are not substantial improvements. As mentioned earlier, despite the ignition timing was retarded from the MBT timing, the change in the amount of useful work by the shift of KLSA was not as sensitive to the change in the ignition timing.

The incomplete combustion loss was increased due to the wall temperature reduction. This can be caused by earlier flame quenching due to cooler walls, poorer fuel vaporization and reduced homogeneity of the air-fuel

mixture. Although the exhaust loss could be reduced at the 60°C coolant temperature case with the use of earlier ignition timing, most of the gain was almost zero-summed by increased cooling loss and incomplete combustion.

In summary, the use of a lower coolant temperature can modestly increase the overall ITE as well under part load conditions where the KLSA equals the MBT timing. The reduction in exhaust loss from the advanced combustion phasing was not equivalent to the increase in work output due to the reduced combustion efficiency and increased cooling loss. The main contribution to the slight increase in useful work can be attributed to reduced compression work.

### 3.2 Estimation of the effect of coolant temperature on heat transfer using 3D simulation

#### 3.2.1 Quantitative comparisons of heat transfer at various stages during a cycle

The heat transfer between the in-cylinder gas and combustion chamber walls is a very complex phenomenon. First, the air entering the combustion chamber receives heat from engine components, as the fresh air generally has a lower temperature than the walls. The temperature difference between the intake air and the walls can be greater in a naturally aspirated engine due to the absence of an additional heat source, such as a turbocharger.

During the early stage in the intake stroke, the air is heated mainly by convective heat transfer from the surfaces, including the intake port, intake valves, and combustion chamber walls. After the IVC timing, the charge begins to be compressed, and the gas temperature increases as a result. At a certain point, the charge temperature exceeds the surrounding wall temperatures, and the direction of heat transfer reverses. This timing where this inversion occurs is defined as ‘inversion timing (IT)’ in this study. While the IT may change depending on the operating condition, the lowered wall temperature achieved by the cooling strategy enhances the heat transfer from the charge to the wall, lowering the charge temperature after the IT. Last, the reduced wall temperatures increase the heat transfer from the hot unburned gas to the walls during the combustion process, which helps mitigate knock.

In brief, the impact of reducing charge temperature by lowering wall temperatures can be categorized into three categories. The first stage (phase 1) is defined from TDC to IT. The second phase (phase 2), where a negative heat transfer occurs after IT, is defined as the period from IT to ignition timing (IGN), and the last stage (combustion, phase 3) is determined as the period from IGN to knock onset (KO).

To investigate the influences of the aforementioned three phases with different cooling strategies, the baseline case and the case with enhanced cooling for both the liner and the head, listed in Table 5, were selected for the simulations. There was a slight difference in IT for each condition, e.g., 85.9 CA bTDC in the baseline case and 91.8 CA bTDC under all cooling conditions. For simplification, the IT was fixed at 85 CA bTDC. This did not introduce much difference in the calculated amount of heat transferred to and from the charge to the walls because the heat transfer rate approaches zero near IT.

Out of three thousand consecutive cycles, approximately 300 cycles were determined to be the knocking cycles. The average KO timing was found to be near 40 CA aTDC by in-house post-processing logic [53]. Thus, 40 CA aTDC was used to define the end of the third phase. During the simulation in the combustion phase (phase 3) at 60°C, the data were replaced with the results of the baseline condition at 5 CA prior to ignition timing to solely investigate the effect during combustion; thereby, the condition until ignition timing could be held constant, and subsequently, the amount of induced air was unchanged during the simulation.

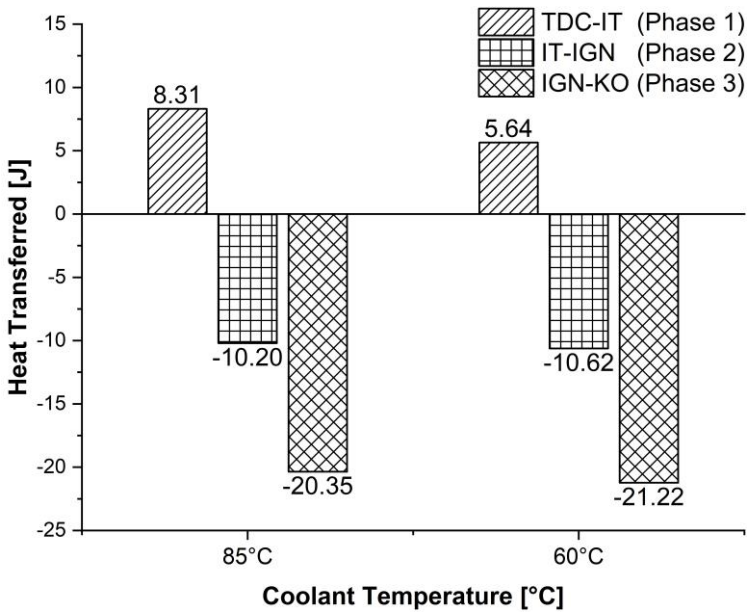


**Fig. 10**. Estimated amount of heat transfer from various stages at 1500 rpm under full load conditions.

Fig. 10 displays the amount of heat transferred from the combustion chamber walls to the charge at various phases for the baseline condition ($T_{cw}$ = 85°C) and enhanced cooling condition ($T_{cw}$ = 60°C). By definition, positive values indicate heat transferred from the walls to the gas, and negative values indicate the opposite.

The difference in heat transfer due to enhanced cooling was significantly larger in phase 1. The total amount of heat added to the charge from the walls decreased by 32.1% when the coolant temperature was reduced. On the other hand, only minor differences were observed at phase 2 (IT-IGN) and phase 3 (IGN-KO) with a reduction in the coolant temperature.

During phase 1, the charge motion is very intense, and the surface areas for the heat transfer are relatively large. Furthermore, the duration of phase 1 is longer than that of the other phases, which allows more time for heat transfer. All of these factors lead to a greater impact of the coolant temperature on the heat added to the charge. In addition, the unburned gas temperature determined at the end of phase 1 increases in the other phases by following the

404 polytropic process. For this reason, a slight change in phase 1 results in a substantial difference in the unburned gas
405 temperatures in phases 2 and 3.

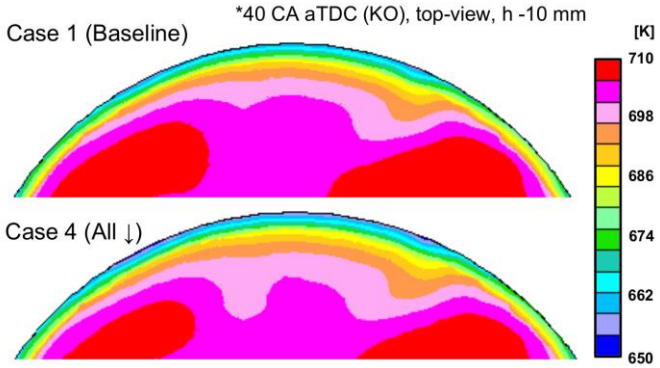


406

407 **Fig. 11**. Unburned gas temperature distribution at the baseline and enhanced cooling conditions.

408 The minor difference in phase 2 is attributed to the shorter period of time available for heat transfer and the
409 reduced surface area of the liner. The results from phase 3 can be explained in a similar manner, although the end
410 gas temperature becomes much higher due to compression from piston movement as well as deflagration. Fig. 11
411 shows a cross-section of the unburned gas temperature distribution during phase 3 for baseline and enhanced cooling
412 conditions. The planar distribution was obtained at the timing of KO (40 CA aTDC) and 10 mm below the top
413 surface of the piston at the TDC position. Only a subtle change, less than a 4 K decrease in average, was observed
414 from the enhanced cooling condition.

415 From the results, it can be concluded that due to the reduced amount of heat transferred from the compressed
416 charge to the walls during phases 2 and 3, the factor that contributes the most to the lower end gas temperature
417 during combustion is the charge temperature at IVC timing. This is because even a small difference in this
418 temperature propagates and is magnified during compression due to the polytropic process. To increase the impact
419 of phases 2 and 3 on lowering the end gas temperature, it is necessary to increase the convective heat transfer

coefficient by enhancing turbulence near the end of compression. This can be realized by optimizing the piston design [28]. A piston design optimized for increasing turbulence at the end of the compression stroke can be an advantageous option to achieve a synergetic effect with the wall cooling strategy in terms of knock mitigation.

### 3.2.2 Heat transfer during the intake stroke and early part of the compression stroke (until IT)

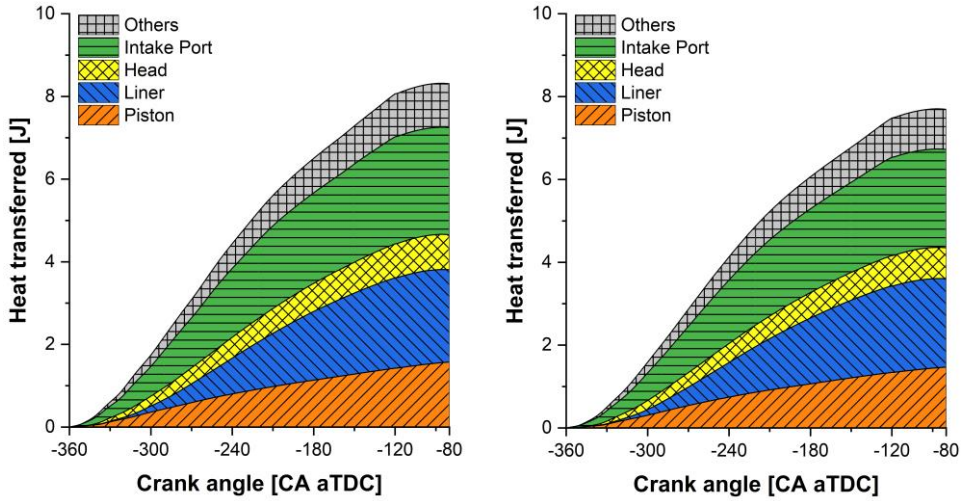


**Fig. 12**. The cumulative amount of heat transferred from various walls to the fresh charge during phase 1 at (a) 1500 rpm, full load and (b) 2000 rpm, full load.

Figure 12 illustrates the cumulative amount of heat transferred from the individual walls to the charge during phase 1 at two engine speeds. The conditions for baseline (case 1) in Table 5 were used in this simulation. Because the wall temperatures were fixed to the values from 1500 rpm, the full load condition, the effect of engine speed and hence differences in the convective heat transfer and time available for heat transfer could be assessed. Near 85 CA bTDC, the cumulative heat transfer approached a plateau, and the heat transfer direction was reversed (IT). The components categorized as “others” in the figure include the spark plug, intake and exhaust valves and intake valve stems.

Not only the temperatures of the intake port wall but also the wall temperatures of the components installed on the head are strongly affected by the head coolant temperature. As shown in Fig. 12, the amount of heat transferred to the head and its components accounts for more than 50% of the total amount at both engine speeds. This finding highlights that enhancing the engine head cooling is an effective way to reduce the charge temperature.

The intake port is identified to be the greatest contributor of adding heat to the inducted air among the components. This finding, first introduced by Imaoka et al. [43], was attributed to the total surface area of the intake port being considerably large and to the relatively high velocity of the flow. Therefore, the addition of intake port insulation was proposed as an effective measure to reduce the charge temperature and mitigate knock [43-45].

A higher engine speed strengthens the in-cylinder flow and turbulence while also reducing the time over which heat transfer takes place. When comparing the results between 1500 and 2000 rpm in the figure, it was found that the total amount of transferred heat was lower at 2000 rpm. This implies that the impact of the reduced time for heat transfer was larger than that of the increased convective heat transfer coefficient. This result agrees well with the scaling law of convective heat transfer [59]: the convection coefficient scales with the engine speed is to the power of 0.8, while the time available for heat transfer is inversely proportional to the engine speed. Therefore, the amount of heat from convective heat transfer scales with the engine speed to the power of -0.2, indicating that the amount of heat transfer decreases with increasing engine speed. Thus, a higher engine speed has better knock resistance due to not only the faster flame speed and less residence time for a shorter ignition delay but also the lower unburned gas temperature if other conditions remain constant.

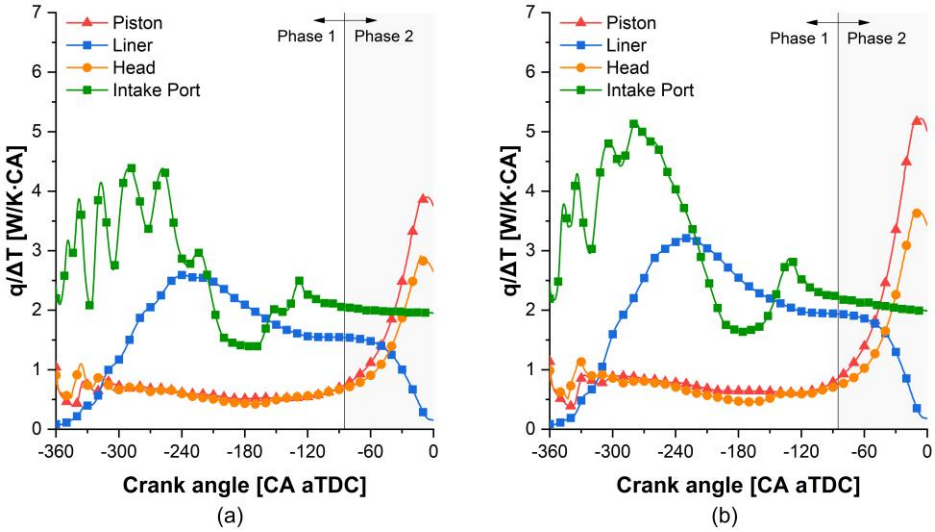


**Fig. 13.** Estimated convective heat transfer rate (q) divided by the average temperature gradient (ΔT) for various surfaces under full load conditions at (a) 1500 rpm and (b) 2000 rpm.

Fig. 13 shows the heat transfer characteristics between the gas exchange TDC (360 CA bTDC) and firing TDC (0 CA aTDC) under full load conditions at 1500 and 2000 rpm. To observe the effect without considering the value and spatial distribution of temperature, the y-axis indicates the rate of convective heat transfer (q) divided by the average temperature gradient (ΔT). Other minor components, such as the spark plug and intake valve stems, are excluded. Compared to the 1500 rpm case, a significant increase in the heat transfer from the liner and intake port to charge was notable in the 2000 rpm case. On the other hand, no remarkable difference in the heat transfer characteristics was found on the piston and head surfaces during phase 1; however, a drastic increase at the end of the compression stroke was observed.

The share of the head components contributing to the added heat transfer to the charge was not significant except for the intake port during phase 1. Considering exclusion of the intake port heat transfer, e.g., intake port insulation, the fraction of the liner and piston composes most of the total heat transfer occurring between the charged air-fuel mixture and wall components. This implies that head cooling may not be the best solution when intake port

insulation is implemented in the engine. Therefore, further study was conducted to observe the impact of different cooling strategies.

### 3.3 Effect of wall temperature variation using a segregated cooling passage

#### 3.3.1 Demonstration of independent wall temperature control

In terms of systemwise engine efficiency, it is not favorable to supply cooler coolant to all of the components because it increases the accessory work and frictional loss due to the high viscosity of the lubricant and heat loss. Therefore, a split cooling strategy has been proposed in numerous studies. Similarly, the effect of enhanced cooling for individual components was investigated using the segregated cooling passages of the cylinder head and liner in this work.

The variations in wall temperatures were demonstrated under independent cooling of each component. The engine test was conducted under consistent conditions: 1500 rpm and 5.96 bar of nIMEP. The coolants of the liner and head were individually controlled. Specifically, while one coolant temperature was adjusted, the temperature of the other coolant was held constant at 85°C. During the test, the ignition timing was adjusted to the MBT timing for each case. In this set of experiments, the KLSA was the same with MBT only when both coolants were 85°C, and other cases showed all knock-free (less than 10%) as the knock was mitigated by enhanced cooling.

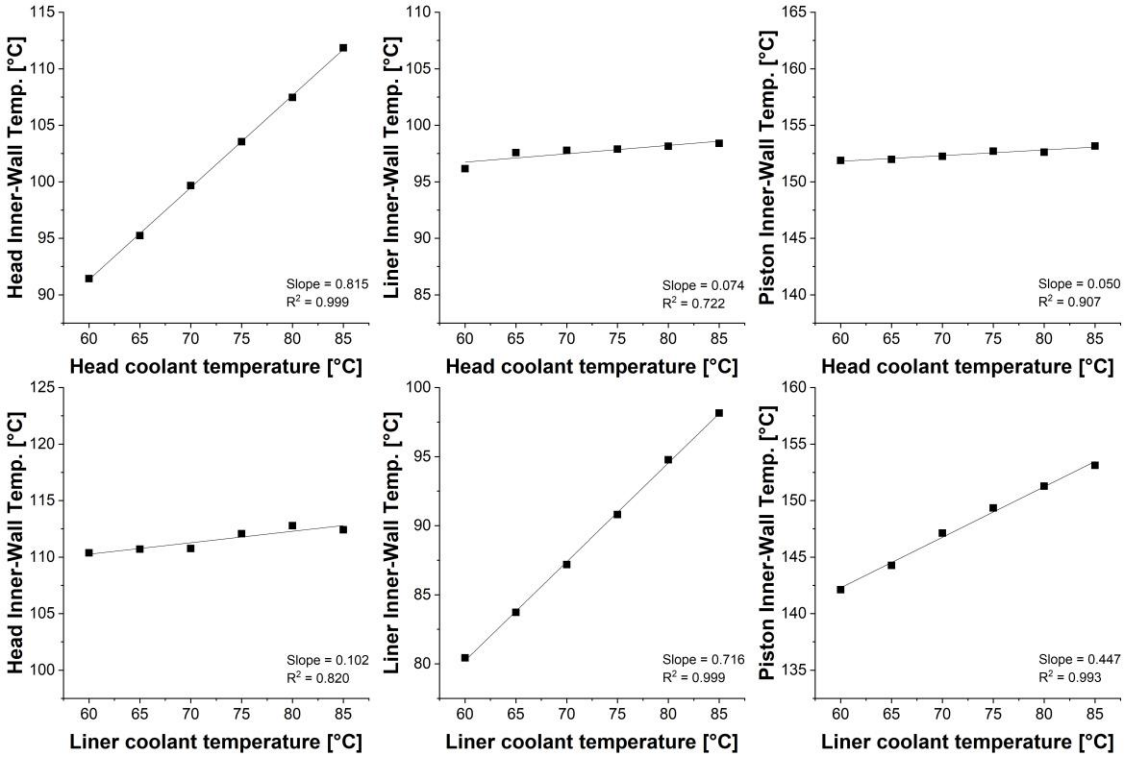


**Fig. 14**. Variations in the inner-wall temperatures of the head, liner and piston according to the change in the coolant temperatures supplied to the head (top) and liner (bottom).

Fig. 14 displays the temperature variation results when the coolant temperatures supplied to the head and liner were changed. The temperatures in the top three figures correspond to the case where the head coolant temperature was varied from 60°C to 85°C while the liner coolant temperature was maintained at 85°C. The temperatures in the bottom half of the figure correspond to the case where the liner coolant temperature was varied while the head coolant temperature was maintained at 85°C. From left to right, the y-axes of the graphs indicate the temperatures of the head surface, liner surface and piston. The axis range is fixed to 35 K in all of the figures.

Notably, the segregated cooling strategy facilitated a nearly independent control of wall temperatures. For instance, when the head coolant temperature was changed, the inner-wall head temperature was mainly affected,

whereas the inner-wall liner and the piston temperatures were not significantly influenced. Conversely, in the liner-control case (bottom three figures), the liner coolant temperature governed the liner inner-wall temperature but did not significantly affect the head inner-wall temperature. Note that the piston temperature was more sensitive to the liner coolant temperature than the head coolant temperature. Considering the slope of the linear regression shown in the figures, the impact of the liner coolant temperature on the piston surface temperature was approximately nine times than that of the head coolant temperature. This is because the piston was in more direct contact with the liner.

### 3.3.2 Effect of the segregated cooling strategy on knock mitigation

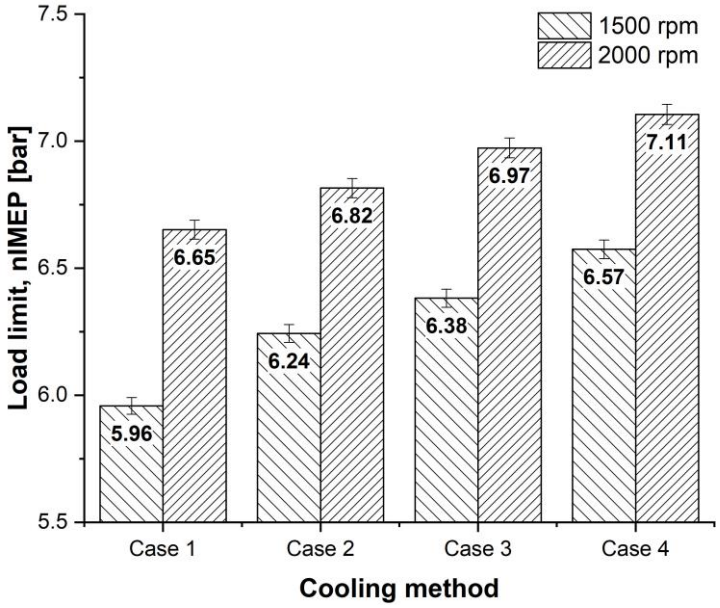


**Fig. 15**. Change in knock-limited nIMEP under various cooling strategies. A coolant temperature of 85°C was used for both head and liner cooling in the baseline case.

Fig. 15 shows the knock-limited nIMEP at various cooling strategies at 1500 and 2000 rpm. A coolant temperature of 85°C was used for the head and liner cooling at the baseline condition. For other cases, the coolant temperature was reduced to 60°C and supplied to either the liner or head or both the liner and the head. The base

condition indicates that the cases of both coolant temperatures were maintained at 85°C, and "Liner 60°C" means the cases in which only the liner coolant temperature decreased to 60°C. During the experiments, the load limit was determined as the maximum achievable load maintaining the KLSA advanced to MBT timing as long as the MAPO incidence did not exceed 10%. Due to enhanced cooling, the maximum load could be increased. From the baseline to simultaneous cooling cases, 10.3% in 1500 rpm and 6.8% in 2000 rpm of the load expansions were obtained by reducing the coolant temperatures by 25 K.

The results reveal that enhanced cooling on the head is more effective than intensified liner cooling. Similar results were shown in the work of Russ [38], Imaoka [43] and Cho [29]. The enhanced head cooling exhibited load limit expansions of approximately 7.1%, whereas the excess liner cooling showed only 4.8% at 1500 rpm. The expansion rate slightly decreased at higher engine speeds. There was a 4.8% improvement in the head 60°C condition and a 2.5% improvement in the liner 60°C condition at 2000 rpm. This is attributed to the reduced time for heat transfer at higher engine speeds, thus restricting the effect of lowering the coolant temperature.

As mentioned previously, knock can be suppressed by changing the heat transfer between the in-cylinder charge and the walls. The results in the previous section suggest that lowering the liner coolant temperature may reduce the charge temperature more. This is because the cooler liner coolant also reduces the piston surface temperature, which results in a larger wetted area for convective heat transfer with lower surface temperature. However, lowering the head coolant temperature was more effective in mitigating knock. Therefore, the fact that lowering the cylinder head temperature has other large impacts was verified, specifically regarding the influence of the intake port.

# 4. An approach for strategic cooling towards higher efficiency

## 4.1 Beyond the intake port insulation

As it was found that the intake port has the most significant role in decreasing the charge temperature using simulations and experiments, it is reasonable to add thermal insulation to the intake port wall to improve the engine knock resistance. Recent studies have proposed and explored various materials, such as plastic [43] or resin and polyphenylene sulfide (PPS) [45], which have remarkably lower thermal conductivity than casted aluminum. In this study, to best capitalize on the available mechanisms, the individual cooling effect in addition to the application of intake port insulation was investigated.

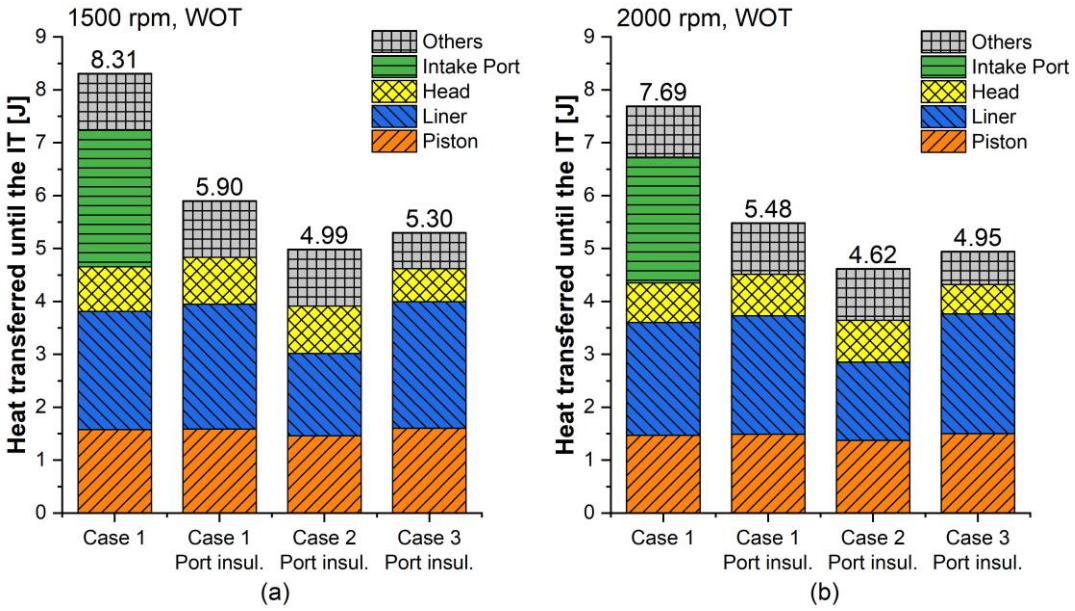


**Fig. 16**. Estimated heat transferred from walls to charge until the IT at (a) 1500 rpm and (b) 2000 rpm.

Fig. 16 shows the estimated heat transferred from individual walls to the charge mixture until the IT in full load conditions under various enhanced cooling strategies. Fig. 16(a) shows the results at 1500 rpm, and Fig. 16(b) shows the results at 2000 rpm. In this study, the wall temperatures were unvaried when the engine speed increased to 2000 rpm to solely investigate the effect of engine speed. Case numbers in this section are explained in the Table. 5, and

wall temperatures of case 1 was obtained from the full load experiment at 1500 rpm as previously described. The values of the baseline cases correspond to the accumulated value at the IT in Fig. 11. Case 2 in the figure indicates that the liner coolant temperature was decreased to 60°C from the baseline, while the head coolant temperature was held at 85°C. Case 3 indicates the opposite case. Case with port insulation means that the case was assumed with additional insulation in the intake ports. During the simulations for the intake port insulation, the heat transfer process in the intake ports was reasonably assumed to be adiabatic to mimic the heat insulation effect.

When the intake port heat transfer was neglected, the heat transferred was drastically reduced by 29% from the baseline level to 5.9 J at 1500 rpm and reduced by 28.7% to 5.48 J at 2000 rpm. The results of demonstrate how large of an effect in the charge temperature reduction is realized with the thermal insulation of the intake port. The heat to the charge from the other components, such as the liner and the piston, was slightly increased due to the reduced charge temperature.

Similar to the results shown in the previous section, the effect of independent cooling was examined at both engine speeds. As shown in both Figures 16(a) and (b), the enhanced liner cooling cases showed more substantial effects on the decrease in heat transfer during phase 1 compared to the enhanced head cooling cases. As discussed, the majority of the impact of the head coolant on heat transfer comes from the intake port surface. Therefore, it was shown that head cooling did not play a significant role when intake port insulation was applied.

The liner cooling (case 2) showed a larger decrease in the heat transferred between the charge and liner (blue color) at both engine speeds. Enhanced liner cooling is found to suppress knock more effectively than increased head cooling, particularly when intake port insulation technology is adopted. This is attributable to the large surface area of the liner as well as the impact of inducted gas that enters the combustion chamber with a high velocity and impinges on the wall during the intake stroke.

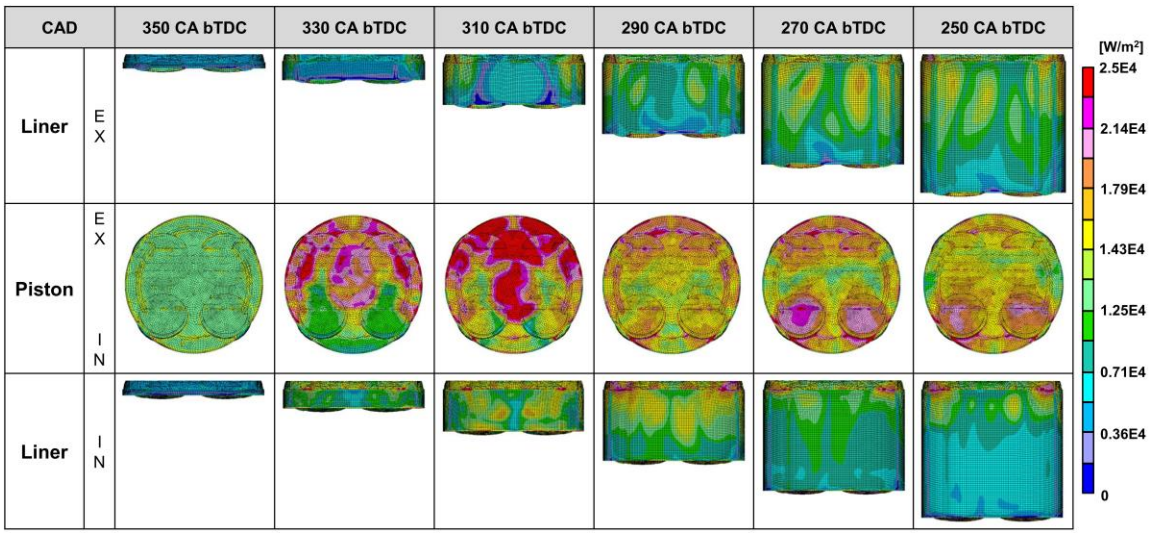


**Fig. 17.** Heat flux on the individual surfaces at 1500 rpm and the full load condition with the heat insulated port.

Fig. 17 illustrates the magnitude of heat flux from the piston and liner to charge during the early stage in the intake process. The figures are arranged in the manner of time flow from left to right. The top figures show the heat flux variations on the exhaust side (EX) of the liner, and the bottom figures show the intake side (IN).

Regarding the early stage in the intake stroke until 310 CA bTDC, the charge hit the cylinder liner wall vigorously on the intake side after it passed the intake valves. In contrast, the charge towards the exhaust side showed no significant heat flux due to the lack of inertia to impinge. However, the exhaust-sided charge produced a downgoing plume and ultimately exhibited substantial heat transfer, so a significant amount of heat flux can be found, particularly on the exhaust side of the piston surface. Even if the majority of heat transfer occurred on the exhaust side of the piston surface, the intake side of the piston surface also showed a considerable magnitude of heat flux at the later stage. Not only the charge entering the chamber but also the charge heading to the exhaust side generated a breaststroke-like motion that intensified the heat flux on the intake side at the later stage during the intake stroke. Subsequently, as the intake charge continuously entered the cylinder, the charge gained momentum to strike the

exhaust-sidewall of the liner; therefore, high heat flux was observed on the exhaust side after 270 CA bTDC with a large surface area.

Takahashi et al. [42] suggested the importance of enhanced cooling on the upper part of the exhaust side of the liner to reduce its large heat transfer to the charge during the intake stroke as well as to reduce the piston ring friction increase by lowering the liner coolant temperature. However, it was found that the intake side of the upper-part liner wall showed a considerable amount of heat transfer to the charge at the earliest stage of the intake process. Therefore, in addition to shortening the combustion duration by an increasing turbulence intensity and tumble ratio, an intensified intake tumble port can be suggested to maximize the effect of the suggested cooling strategy, as it would let the charge flow mainly towards the exhaust side and thus maximize the effect of enhanced liner cooling.

### 4.2 Effect of an intensified tumble port

The most common approach to realize enhanced tumble motion and increased turbulence intensity is to adopt intake port geometries to intensify tumble motion. In this work, variations in the heat transfer characteristics as well as the effect of enhanced liner cooling were investigated when the intensified tumble port was adopted. The simulations were conducted at 1500 rpm under full load conditions.

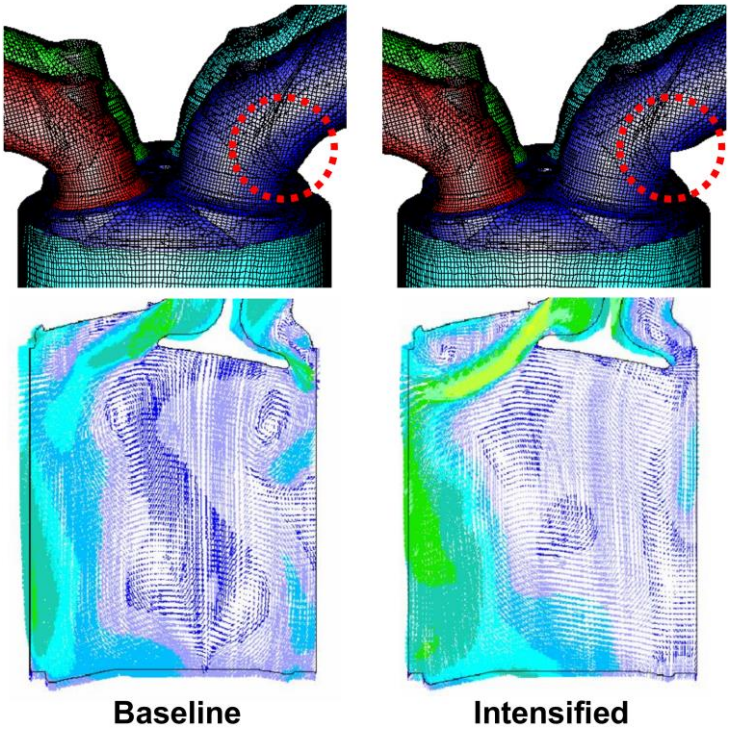


**Fig. 18**. Comparison of normal intake ports (baseline) and intensified intake ports.

Fig. 18 shows the intake port designs used in this study. The altered design to implement the intensified port has a typical jump ramp (shown in the red circles) to direct the intake air flow towards the exhaust side. In the figures, the increased velocity magnitude of intake air flow during the intake process (at 240 CA bTDC) can be observed in the figure. In the baseline condition, the charge collision to the intake side is observable, as mentioned in the previous section. For the simulation process, the trapped mass was constant.

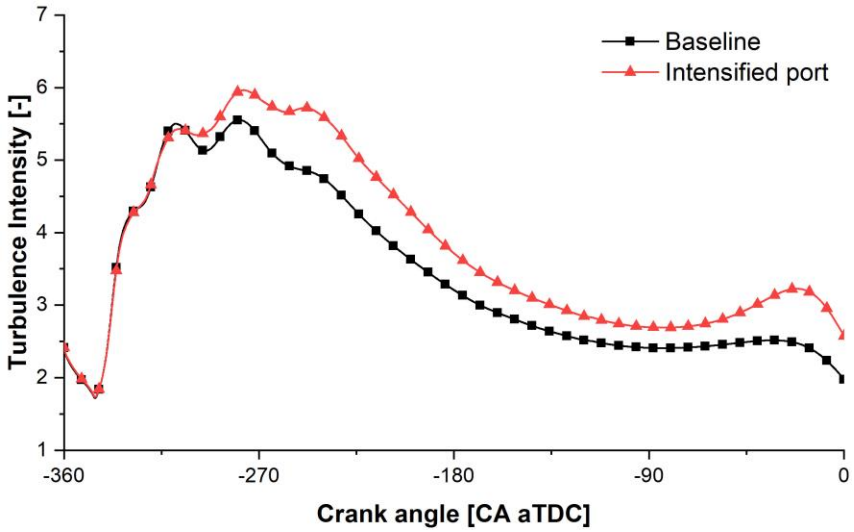


**Fig. 19**. Turbulence intensity enhancement from the modified intake port design.

Fig. 19 displays the change in the turbulence intensity when the intake port design was modified for stronger tumbles. It is confirmed that the modified intake port design works well to enhance both the intake air velocity and the turbulence intensity. The recovery of turbulence intensity at the end of compression stroke was notable in the intensified port case.

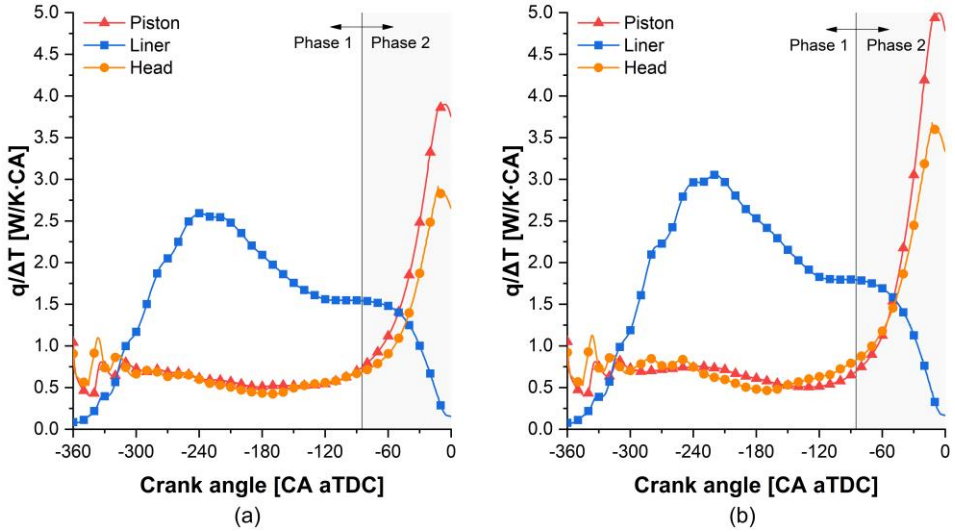


**Fig. 20**. Estimated convective heat transfer rate (q) divided by the average temperature gradient (ΔT) for various surfaces at the (a) baseline and (b) intensified port.

In Fig. 20, the estimated convective heat transfer rates (q) divided by the average temperature gradient (ΔT) depending on the individual components are shown. Assuming the temperature of the charge is uniform, the heat transfer from the liner wall to the charge increased during the intake stroke when the intensified port was applied. The impacts of other parts remained at a similar level during phase 1 (TDC to IT). However, the intensified ports showed a higher rising rate of the piston and head values after the IT. This means that more heat was transferred from the charge to the wall, which was beneficial to reduce the unburned gas temperature. This is attributable to the elevated turbulence intensity at the end of the compression stroke.

It can be counterintuitive that intensified tumble motion has the advantage of reducing the charge temperature in the early stage but may increase the heat loss during the combustion. The large-scale motion by the tumble diminishes near TDC, and the production rate of the turbulence significantly decreases due to the volume expansion process of the expansion stroke [60]. Therefore, the convective heat transfer coefficient also drastically decreases. Due to this, the heat transfer loss during the combustion would not show a substantial change when an intensified

615 tumble port is adopted. In addition, it has already been shown from previous studies that intensified tumble port has
616 a remarkable effect on increasing the thermal efficiency.

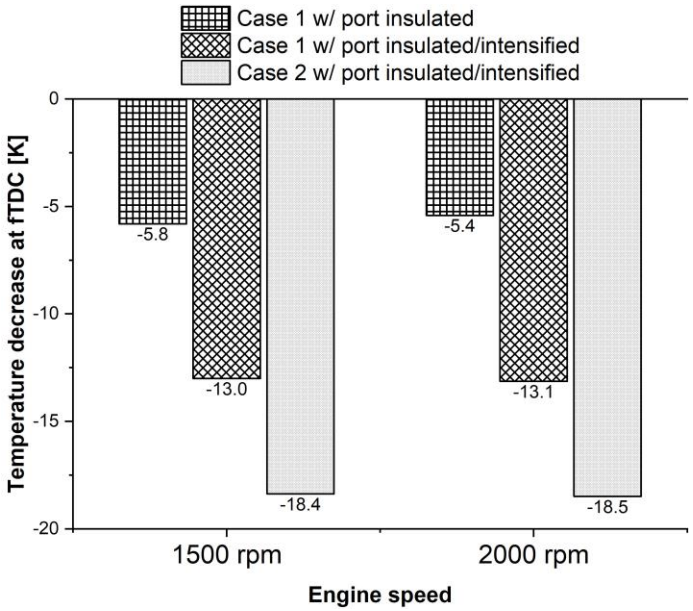


617

618 **Fig. 21**. Estimated reduction in charge temperature at fTDC for various strategies.

619 Fig. 21 shows the estimated reduction in charge temperature achieved by the proposed strategies. The simulation
620 was implemented without combustion. While the port insulation showed a 5-6 K decrease in the estimated
621 temperature at firing TDC (fTDC), the additional port insulation showed an extraordinary additional effect: an
622 approximately 13 K drop for both engine speeds. This indicates that the elevated heat transfer from charge to the
623 walls after the IT was larger enough to cancel all of the disadvantage from the increased heat transfer in phase 1. As
624 the enhanced liner cooling (case 2) became more substantial by the intensified flow, liner cooling was more
625 preferable in these circumstances and showed more than 18 K of reduction in temperature at fTDC in both the 1500
626 and 2000 rpm cases.

Therefore, from the results, it can be concluded that a high tumble design exploits the reduction in the charge temperature by increasing the convective heat transfer from charge to the chamber walls during compression, even though a disadvantage arises regarding the gas temperature increment in the gas induction phase. Moreover, this approach shows high compatibility with an enhanced liner cooling strategy. From the observations, it is concluded that the most favorable engine design for knock suppression is one that lowers the gas speed during the intake process to decrease the heat addition to the charge but enhances the tumble ratio and turbulence again in the compression stroke. On top of that, the turbulence dissipation also will contribute to the increase in charge temperature, and this will become more significant in higher speed and intensified port conditions. A further investigation is still required to decouple this effect from the result. However, as low-end torque region with low turbulence is more knock-prone, so the wall-charge heat interaction would still take a valuable portion.

Considering a large heat loss of the single-cylinder engine used in this study, multi-cylinder engines will show higher wall temperatures. The higher wall temperatures of a multi-cylinder engine will make the liner wall's impact more significant than what was shown in this study. The suggested strategy with enhanced liner cooling will be even more effective for knock mitigation because of the direct relationship in temperatures between piston surface and liner wall. However, additional cooling needs a higher accessory work. Although increased ITE was shown in this study and a strategic cooling was proposed, it still needs a follow-up study to fully adopt the suggested strategy to multi-cylinder engines.

It is a noticeable trend that most gasoline engines are equipped with gasoline direct injection (GDI) systems to achieve high thermal efficiency and additional charge cooling effect. In a knock-prone high-load region, the engine can gain a better mixture homogeneity due to its high wall temperature and more vigorous flow motion, so the effect of enhanced liner cooling described in the study would not be deteriorated [29]. Furthermore, increasing the stroke-to-bore ratio for higher thermal efficiency is making the surface area ratio of liner wall larger, therefore decreasing

liner wall temperature is expected to be more favorable. From ideas and suggestions above, increasing studies are required.

## 5. Conclusion

In this study, a systematic approach was demonstrated to investigate the impact of engine wall temperatures on the knock phenomenon. A refined engine experiment with high-fidelity data was conducted by varying the coolant temperatures, and 3D simulation was also employed and provided a deeper understanding of heat transfer by dividing the phases. Moreover, dissections of fuel energy balance were made to observe the energy flow using 0D-based combustion analysis. Under the given approaches, the interaction of temperatures between the unburned gas, engine walls and coolants was analyzed under various conditions. Accordingly, strategic cooling methods were suggested for higher engine efficiency based on the results. The summary of this work is the following conclusions:

1. The engine experimental results showed that an enhanced cooling strategy can effectively suppress knock by reducing the charge temperature, leading to an improvement in the thermal efficiency. In the full load condition, a significant amount of exhaust loss heat was recovered with an increased combustion speed and advanced combustion phasing. In the part load condition, the gross work was increased by the reduced in-cylinder pressure during the compression stroke despite no significant increase in the expansion work.
2. Using 3D CFD simulation, it was found that the first phase, i.e., the period during the intake stroke until the inversion timing, had the most critical impact on the convective heat transfer when enhanced cooling was applied. In terms of later phases, i.e., compression and combustion periods, to further mitigate knock, it is suggested to enhance the heat transfer with suitable designs to decrease the charge temperature, and an optimal piston design is recommended.

3. The intake port showed a remarkable portion of the heat transfer between the charge gas and walls during the intake process. At this point, thermal insulation in the intake port wall can favorably affect the engine performance. It was found that enhanced cooling on the liner could be more effective than head cooling when thermal insulation is applied to the intake port wall due to the large effective surface area of the liner and piston.
4. The intensified intake port also showed a large advantage in decreasing the unburned gas temperature by enhancing convective heat transfer from the charge to the wall after the inversion timing. In terms of the temperature at firing top dead center, the enhanced cooling on liners with intensified/insulated intake ports showed more than 18 K of reduction. The enhanced liner cooling became significant for knock mitigation.

## 6. Acknowledgments

This work was made possible by the unconditional support of research fellow Dr. Kyoung-pyo Ha and senior researchers Backsik Kim and Ingee Suh of Hyundai Motor Company. The test facility was supported by the Advanced Automotive Research Center (AARC) and Institute of Advanced Machinery and Design (IAMD) of Seoul National University. The authors would like to express their sincere gratitude to these groups.

## 7. References

[1] Wang Z, Liu H, and Reitz RD. Knocking combustion in spark-ignition engines. Progress in Energy and Combustion Science. 2017;61:78-112. https://doi.org/10.1016/j.pecs.2017.03.004.

[2] Reducing CO2 emissions from passenger cars. European Committee. "https://ec.europa.eu/clima/policies/transport/vehicles/cars_en". Access date: Feb 22, 2022.

[3] Heywood JB. Internal Combustion Engine Fundamentals. New York: McGraw-Hill; 1988.

[4] Hwang K, Hwang I, Lee H, Park H, et al. Development of New High-Efficiency Kappa 1.6L GDI Engine.

690 SAE Technical Paper 2016-01-0667. 2016. https://doi.org/10.4271/2016-01-0667.

691 [5] Niizato T, Yasui Y, Urata Y, Wada Y, et al. Honda's New Turbo-GDI Engine Series for global application.
692 37th International Vienna Motor Symposium. 2016.

693 [6] Ikeya K, Takazawa M, Yamada T, Park S, et al. Thermal efficiency enhancement of a gasoline engine. SAE
694 International Journal of Engines. 2015;8:1579-86. http://doi.org/10.4271/2015-01-1263.

695 [7] Omura T, Nakata K, Yoshihara Y, and Takahashi D. Research on the Measures for Improving Cycle-to-Cycle
696 Variations under High Tumble Combustion. SAE Technical Paper 2016-01-0694. 2016.
697 http://doi.org/10.4271/2016-01-0694.

698 [8] Yoshihara Y, Nakata K, Takahashi D, Omura T, et al. Development of High Tumble Intake-Port for High
699 Thermal Efficiency Engines. SAE Technical Paper 2016-01-0692. 2016. http://doi.org/10.4271/2016-01-0692.

700 [9] Takahashi D, Nakata K, Yoshihara Y, and Omura T. Combustion development to realize high thermal
701 efficiency engines. SAE International Journal of Engines. 2016;9:1486-93. http://doi.org/10.4271/2016-01-
702 0693.

703 [10] Nakata K, and Shimizu R. Toyota's new combustion technology for high engine thermal efficiency and
704 high engine output performance. 37th International Vienna Motor Symposium. 2016.

705 [11] Adachi S, and Hagihara H. The Renewed 4-Cylinder Engine Series for Toyota Hybrid System. 33th
706 International Vienna Motor Symposium. 2012.

707 [12] Lee B, Oh H, Han S, Woo S, et al. Development of High Efficiency Gasoline Engine with Thermal
708 Efficiency over 42%. SAE Technical Paper 2017-01-1229. 2017. http://doi.org/10.4271/2017-01-2229.

709 [13] Schenk M, Wolf T, Schröter M, Zellinger F, et al. Corona-Ignition vs. Spark Ignition: A Fundamental
710 Comparison for varying thermodynamic conditions of modern turbocharged Gasoline Engines. SIA Powertrain
711 Conference. 2015.

712 [14] Attard WP, Kohn J, and Parsons P. Ignition Energy Development for a Spark Initiated Combustion System
713 Capable of High Load, High Efficiency and Near Zero NOx Emissions. SAE International Journal of Engines.
714 2010;3:481-96. https://doi.org/10.4271/2010-32-0088.

715 [15] Cathey CD, Tang T, Shiraishi T, Urushihara T, et al. Nanosecond Plasma Ignition for Improved
716 Performance of an Internal Combustion Engine. IEEE Transactions on Plasma Science. 2007;35:1664-8.
717 http://doi.org/10.1109/TPS.2007.907901.

718 [16] Toulson E, Schock HJ, and Attard WP. A Review of Pre-Chamber Initiated Jet Ignition Combustion
719 Systems. SAE Technical Paper 2010-01-2263. 2010. https://doi.org/10.4271/2010-01-2263.

[17] Kim N, Vuilleumier D, Sjöberg M, Yokoo N, et al. Using Chemical Kinetics to Understand Effects of Fuel Type and Compression Ratio on Knock-Mitigation Effectiveness of Various EGR Constituents. SAE Technical Paper 2019-01-1140. 2019. https://doi.org/10.4271/2019-01-1140.

[18] Duva BC, Wang Y-C, Chance L, and Toulson E. The Effect of Exhaust Gas Recirculation (EGR) on Fundamental Characteristics of Premixed Methane/Air Flames. SAE Technical Paper 2020-01-0339. 2020. https://doi.org/10.4271/2020-01-0339.

[19] Zahedi P, and Yousefi K. Effects of pressure and carbon dioxide, hydrogen and nitrogen concentration on laminar burning velocities and NO formation of methane-air mixtures. Journal of Mechanical Science and Technology. 2014;28:377-86. http://doi.org/10.1007/s12206-013-0970-5.

[20] Zhuang Y, Qian Y, and Hong G. The effect of ethanol direct injection on knock mitigation in a gasoline port injection engine. Fuel. 2017;210:187-97. https://doi.org/10.1016/j.fuel.2017.08.060.

[21] Lecointe B, and Monnier G. Downsizing a Gasoline Engine Using Turbocharging with Direct Injection. SAE Technical Paper 2003-01-0542. 2003. https://doi.org/10.4271/2003-01-0542.

[22] Kuwahara K, Ueda K, and Ando H. Mixing Control Strategy for Engine Performance Improvement in a Gasoline Direct Injection Engine. SAE Technical Paper 980158. 1998. https://doi.org/10.4271/980158.

[23] Yang J, and Anderson RW. Fuel Injection Strategies to Increase Full-Load Torque Output of a Direct-Injection SI Engine. SAE Technical Paper 980495. 1998. https://doi.org/10.4271/980495.

[24] Pang HH, and Brace CJ. Review of engine cooling technologies for modern engines. Proceedings of the Institution of Mechanical Engineers, Part D: Journal of Automobile Engineering. 2004;218:1209-15. http://doi.org/10.1243/0954407042580110.

[25] Kobayashi H, Yoshimura K, and Hirayama T. A study on dual circuit cooling for higher compression ratio. SAE Technical Paper 841294. 1984. https://doi.org/10.4271/841294.

[26] Fukuda Y, Tawa H, and Makise A. Increase of Knock Limit in Outboard Motor Through Employment of Dual Control Direct Cooling System. HONDA R AND D TECHNICAL REVIEW. 2004;16:121-6.

[27] Rehman A, Sarviya R, Dixit S, and Pandey RK. Influence of coolant temperature on the performance of a four stroke spark ignition engine employing a dual circuit cooling system. Agricultural Engineering International: CIGR Journal. 2010;12.

[28] Matsuo S, Ikeda E, Ito Y, and Nishiura H. The New Toyota Inline 4 Cylinder 1.8L ESTEC 2ZR-FXE Gasoline Engine for Hybrid Car. SAE Technical Paper 2016-01-0684. 2016. https://doi.org/10.4271/2016-01-0684.

[29] Cho S, Song C, Oh S, Min K, et al. An Experimental Study on the Knock Mitigation Effect of Coolant and

751 Thermal Boundary Temperatures in Spark Ignited Engines. SAE Technical Paper 2018-01-0213. 2018.
752 http://doi.org/10.4271/2018-01-0213.

753 [30] Kubozuka T, Ogawa N, Hirano Y, and Hayashi Y. The Development of Engine Evaporative Cooling System.
754 SAE Technical Paper 870033. 1987. https://doi.org/10.4271/870033.

755 [31] Clough MJ. Precision Cooling of a Four Valve per Cylinder Engine. SAE Technical Paper 931123. 1993.
756 https://doi.org/10.4271/931123.

757 [32] Finlay I, Gallacher G, Biddulph T, and Marshall R. The Application of Precision Cooling to the Cylinder-
758 Head of a Small, Automotive, Petrol Engine. SAE Technical Paper 880263. 1988.
759 https://doi.org/10.4271/880263.

760 [33] Iwashita Y, Kanda M, Hartagiri H, and Yokoi Y. Improvement of Coolant Flow for Reducing Knock. I
761 Mech E Autotech Conference. 1989.

762 [34] Nishino T, Senba H, and Murakami N. Study of engine cooling technologies for knock suppression in spark
763 ignition engines. Mitsuhibishi Motors Technical Review. 2004.

764 [35] Shibata M, kawamata M, Komatsu H, Maeyama K, et al. New 1.0L I3 Turbocharged Gasoline Direct
765 Injection Engine. SAE Technical Paper 2017-01-1029. 2017. https://doi.org/10.4271/2017-01-1029.

766 [36] Sanders J, and Peters M. The Effects of High Temperature of the Cylinder Head on the Knocking Tendency
767 of an Air-Cooled Engine Cylinder. AIRCRAFT ENGINE RESEARCH LAB CLEVELAND OH; 1945.

768 [37] Shiga S, Heywood JB, and Chun KM. Variation of Knocking Characteristics with the Chamber Wall
769 Temperature in a Spark-Ignition Engine. Nihon Kikai Gakkai Ronbunshu, B Hen/Transactions of the Japan
770 Society of Mechanical Engineers, Part B. 1990;56:3193-8.

771 [38] Russ S. A Review of the Effect of Engine Operating Conditions on Borderline Knock. SAE Technical
772 Paper 960497. 1996. https://doi.org/10.4271/960497.

773 [39] Asif M, Giles K, Lewis A, Akehurst S, et al. Influence of Coolant Temperature and Flow Rate, and Air
774 Flow on Knock Performance of a Downsized, Highly Boosted, Direct-Injection Spark Ignition Engine. SAE
775 Technical Paper 2017-01-0664. 2017. http://doi.org/10.4271/2017-01-0664.

776 [40] Cho S, Song C, Min K, Kim M, et al. The Effect of Thermal Boundary Conditions on Knock
777 Charatcteristics in a Single Cylinder Spark Ignited Engine. SIA Powertrain Conference. 2017.

778 [41] Perrone D, Falbo L, Castiglione T, and Bova S. Knock Mitigation by Means of Coolant Control. SAE
779 Technical Paper 2019-24-0183. 2019. https://doi.org/10.4271/2019-24-0183.

780 [42] Takahashi D, Nakata K, and Yoshihara Y. Engine Thermal Control for Improving the Engine Thermal

781 Efficiency and Anti-Knocking Quality. SAE Technical Paper 2012-01-0377. 2012. http://doi.org/10.4271/2012-
782 01-0377.

783 [43] Imaoka Y, Shouji K, Inoue T, and Noda T. A Study of Combustion Technology for a High Compression
784 Ratio Engine: The Influence of Combustion Chamber Wall Temperature on Knocking. SAE International
785 Journal of Engines. 2016;9:768-76. http://doi.org/10.4271/2016-01-0703.

786 [44] Inoue Y, Morioka R, Sato K, Higashi H, et al. Effects of heat transfer in intake ports on engine performance.
787 JSAE 20185297. 2018.

788 [45] Morioka R, Inoue Y, Kojima M, Hoshiba Y, et al. Effects of heat transfer in intake ports on engine
789 performance (Second report). JSAE 20185298. 2018.

790 [46] Uozumi H, Kawamura Y, Matsuki H, Ikeda T, et al. Low-heat-transfer Combustion Chamber for
791 Improvement of Knocking. JSAE 20185348. 2018.

792 [47] Kevric A, Iwamuro M, Richardson P, Kaneta H, et al. Realizing Mixture Formation Benefits with a Dual
793 Port Fuel Injection (PFI) System. SIA Powertrain Conference. 2017.

794 [48] Zhao F-Q, Yoo J-H, and Lai M-C. The spray characteristics of dual-stream port fuel injectors for
795 applications to 4-valve gasoline engines. SAE Technical Paper 952487. 1995. https://doi.org/10.4271/952487.

796 [49] Genin C. Multi-Port Injection (MPI): Combustion Efficiency Improvement and PN reduction. SIA
797 Powertrain Conference. 2017.

798 [50] Michigan Scientific Corporation. CompRatio-D3. 05-4-17 Rev. A.

799 [51] Cho S. Study on the Effect of Cylinder Wall Temperatures on Knock Characteristics in Spark-Ignited
800 Engine. 2018.

801 [52] Gao X, Richard S, Chris H, and Ian B. The Detection and Quantification of Knock in Spark Ignition
802 Engines. SAE Technical Paper 932759. 1993. https://doi.org/10.4271/932759.

803 [53] Cho S, Park J, Song C, Oh S, et al. Prediction Modeling and Analysis of Knocking Combustion using an
804 Improved 0D RGF Model and Supervised Deep Learning. Energies. 2019;12:844.
805 http://doi.org/10.3390/en12050844.

806 [54] Angelberger C, Poinsot T, and Delhay B. Improving Near-Wall Combustion and Wall Heat Transfer
807 Modeling in SI Engine Computations. SAE Technical Paper 972881. 1997. https://doi.org/10.4271/972881.

808 [55] French CCJ, and Atkins KA. Thermal Loading of a Petrol Engine. Proceedings of the Institution of
809 Mechanical Engineers. 1973;187:561-73. https://doi.org/10.1243/PIME_PROC_1973_187_054_02.

[56] Song HH, Padmanabhan A, Kaahaaina NB, and Edwards CF. Experimental study of recompression reaction for low-load operation in direct-injection homogeneous charge compression ignition engines with n-heptane and i-octane fuels. International Journal of Engine Research. 2009;10:215-29. https://doi.org/10.1243/14680874JER03309.

[57] Cho S, Oh S, Song C, Shin W, et al. Effects of Bore-to-Stroke Ratio on the Efficiency and Knock Characteristics in a Single-Cylinder GDI Engine. SAE Technical Paper. 2019. 10.4271/2019-01-1138.

[58] Oh S, Cho S, Seol E, Song C, et al. An Experimental Study on the Effect of Stroke-to-Bore Ratio of Atkinson DISI Engines with Variable Valve Timing. 2018;11(6):1183-93. https://doi.org/10.4271/2018-01-1419.

[59] Woschni G. A Universally Applicable Equation for the Instantaneous Heat Transfer Coefficient in the Internal Combustion Engine. SAE Technical Paper 670931. 1967. https://doi.org/10.4271/670931.

[60] Kim N. A Study on Phenomenological Quasi-Dimensional Combustion Modeling of Spark-Ignited Engine. 2016.

## 8. Appendix A

**Table A1**. Experimental results in full load and part load conditions

| Engine speed [rpm] | 1500 | | | | 2000 | | | |
|---|---|---|---|---|---|---|---|---|
| Load condition | Full load | | Part load | | Full load | | Part load | |
| Coolant temp. [°C] | 85 | 60 | 85 | 60 | 85 | 60 | 85 | 60 |
| Intake pressure [bar] | 1.01 | 1.01 | 0.82 | 0.80 | 1.01 | 1.01 | 0.88 | 0.86 |
| Ignition timing (KLSA) [CA bTDC] | -0.4 | 2.0 | 15.9 | 19.8 | 3.3 | 4.9 | 19.8 | 23.5 |
| CA10-90 [CA] | 27.6 | 24.2 | 19 | 17.3 | 28.6 | 26.3 | 19.2 | 17.8 |
| CA 50 [CA aTDC] | 32.1 | 28.7 | 11.7 | 7.6 | 29.5 | 27.1 | 10.2 | 6.7 |
| nIMEP [bar] | 8.82 | 9.39 | 6.54 | 6.57 | 9.33 | 9.73 | 7.06 | 7.11 |
| gIMEP [bar] | 8.94 | 9.51 | 6.88 | 6.94 | 9.55 | 9.96 | 7.43 | 7.49 |
| PMEP [bar] | 0.12 | 0.12 | 0.34 | 0.36 | 0.22 | 0.23 | 0.37 | 0.38 |
| Fuel [mg/cycle] | 31.78 | 32.67 | 20.94 | 20.94 | 32.68 | 33.33 | 22.30 | 22.30 |
| Exhaust temp. [°C] | 711.8 | 694.5 | 609.4 | 591.3 | 748.8 | 735.9 | 653.5 | 646.8 |
| Comp. work [J] | -189.5 | -189.6 | -126 | -123.4 | -194.9 | -195.3 | -135.7 | -133.9 |
| Exp. work [J] | 616.0 | 644.6 | 457.7 | 457.9 | 650.0 | 670.5 | 493.3 | 494.4 |
| Net work [J] | 440.9 | 469.4 | 327.1 | 328.6 | 466.4 | 486.2 | 353.1 | 355.1 |
| ISFC [g/kWh] | 259.5 | 250.6 | 230.5 | 229.5 | 252.3 | 246.8 | 227.3 | 226.1 |